Three-dimensional Lagrangian Tracer Modelling in Wadden Sea Areas

Diploma thesis by Frank Wolk
Carl von Ossietzky University Oldenburg

Hamburg, October 3, 2003

Contents

List of Figures

List of Tables

Chapter 1

Introduction

In this study, a three-dimensional baroclinic turbulence model especially developed for the simulation of currents and transports in shallow water sea areas (such as the North Frisian Wadden Sea) is extended to include the advective and diffusive transport of passive Lagrangian tracers. In physical oceanography, a tracer is a substance such as a dye or a radioactive isotope that can be traced as it is transported with the mean flow field. The measurement of anthropogenic and natural tracers in the ocean provided the first estimate about the time scales of the ventilation of the deep ocean. Since the 1970s, tracer methods have made significant contributions to the understanding of the ocean circulation, internal water mass structures and time scales of the ventilation. Furthermore, numerical simulations of tracer transport are a valuable tool to estimate the dispersion of pollutants such as oil or sewage disposals in the ocean for the research of the long-term effects and the development of effective counter-active measures.
Advective processes play a key role in the transport of tracer particles, therefore a particle tracking model should resolve these processes as accurate as possible. In this thesis, the analytical solution of the Lagrangian advection equation (*Duwe* [1988]) is used to implement a Lagrangian tracer model. In addition to advection, transport occurs due to turbulent motions in the water column. Turbulent mixing is included in the particle tracking model by means of a stochastic model. The first stochastic model to describe natural phenomena was introduced by Einstein as he studied the random motion of microscopic particles suspended in a fluid (*Einstein* [1905]). Since that time stochastic or random walk models of particle motions have proved to be a successful and flexible tool in the investigation of the dispersion of passive tracers in high Reynolds-number turbulence (*Maier-Reimer and Sündermann* [1982], *Dimou and Adams* [1993], *Hunter et al.* [1993]). Being

Lagrangian in concept, they provide a more natural approach to model turbulent diffusion than differential transport equations.
The following report is structured as follows. The second chapter gives an overview of the numerics and physics of the General Estuarine Transport Model (GETM) and the Lagrangian transport model. In chapter three, results are presented from numerical experiments carried out under idealised conditions. Chapter four shows a realistic application of the three-dimensional transport model to the Wadden Sea area in order to determine the residence time of the Langeoog inter-tidal basin. The summary and an outlook can be found in chapter five. In Appendix A, the analytical solution of the tracer trajectories for the test case described in section 2.1 is derived.

Chapter 2

Theory

2.1 The physics and numerics of GETM

2.1.1 Equations of motion

The General Estuarine Transport Model (GETM) is based on the three-dimensional hydrostatic equations of motions with the Boussinesq approximation and the eddy viscosity assumption (*Haidvogel and Beckmann* [1999]). The horizontal velocity components can be written in Cartesian coordinates as (*Burchard and Bolding* [2002])

$$\begin{aligned}&\frac{\partial u}{\partial t}+\frac{\partial(uw)}{\partial z}-\frac{\partial}{\partial z}\left((\nu_t+\nu)\frac{\partial}{\partial z}u\right)\\&\quad+\alpha\left(\frac{\partial(u^2)}{\partial x}+\frac{\partial(uv)}{\partial y}-\frac{\partial}{\partial x}\left(2A_h^M\frac{\partial u}{\partial x}\right)\right.\\&\quad\left.-\frac{\partial}{\partial y}\left(A_h^M\left(\frac{\partial u}{y}+\frac{\partial v}{\partial x}\right)\right)-fv-\int_z^\zeta\frac{\partial b}{\partial x}\,dz'\right)=-g\frac{\partial\zeta}{\partial x}\end{aligned}\tag{2.1.1}$$

$$\begin{aligned}&\frac{\partial v}{\partial t}+\frac{\partial(vw)}{\partial z}-\frac{\partial}{\partial z}\left((\nu_t+\nu)\frac{\partial v}{\partial z}\right)\\&\quad+\alpha\left(\frac{\partial(vu)}{\partial x}+\frac{\partial(v^2)}{\partial y}-\frac{\partial}{\partial y}\left(2A_h^M\frac{\partial v}{\partial y}\right)\right.\\&\quad\left.-\frac{\partial}{\partial x}\left(A_h^M\left(\frac{\partial u}{\partial y}+\frac{\partial v}{\partial x}\right)\right)+fu-\int_z^\zeta\frac{\partial b}{\partial y}\,dz'\right)=-g\frac{\partial\zeta}{y}.\end{aligned}\tag{2.1.2}$$

Since the vertical velocity equation is included in terms of the so-called continuity equation

$$\frac{\partial u}{\partial x} + \frac{\partial v}{\partial y} + \frac{\partial w}{\partial z} = 0, \tag{2.1.3}$$

it is easy to assure conservation of mass and free surface elevation. In the above equations, u, v and w are the mean velocity components with respect to the x-, y- and z-direction. The x-axis is oriented east-west with positive x towards the west, and the y-axis is oriented south-north with positive y towards the north. The vertical coordinate z is oriented positive upwards and the water column ranges from the bottom $-H(x, y)$ to the surface $\zeta(x, y, t)$ with t denoting time. The diffusion of momentum is described by the kinematic viscosity ν while ν_t as the vertical eddy viscosity refers to the internal friction which is generated as laminar flow becomes irregular and turbulent. The horizontal mixing is parametrised by terms containing the horizontal eddy viscosity A_h^M. The Coriolis parameter and the gravitational acceleration are denoted by f and g, respectively. The buoyancy b is defined as

$$b = -g\frac{\rho - \rho_0}{\rho_0} \tag{2.1.4}$$

where ρ is the density and ρ_0 stands for a reference density. In Eq. (2.1.1) and (2.1.2) the last term on the left-hand side is the internal pressure gradient (due to density gradients) and the term on the right-hand side represents the external pressure gradient which occurs due to surface slopes.
Since the model was specifically developed for simulating currents and transports in coastal domains and estuaries, the drying and flooding of mud flats is incorporated into the governing equations through the coefficient α

$$\alpha = \min\left\{1, \frac{D - D_{min}}{D_{crit} - D_{min}}\right\}. \tag{2.1.5}$$

In the event of drying, the water depth D tends to a minimum value D_{min} and α approaches zero. If $D \leq D_{min}$, the equations of motion are simplified because effects like rotation, advection and horizontal mixing are neglected. This ensures the stability of the model and prevents it from producing unphysical negative water depths. For $D \geq D_{crit}$, α equals unity and the usual momentum equations are retained. In typical Wadden Sea applications, D_{crit} is of the order of 0.1 m and $D_{\min}$ of the order of 0.02 m (see *Burchard* [1998]).

2.1.2 Boundary conditions

At the free surface $z = \zeta(x, y, t)$ and at the bottom $z = -H(x, y)$ kinematic boundary conditions are chosen such that particles move along these boundaries

$$w = \frac{\partial \zeta}{\partial t} + u\frac{\partial \zeta}{\partial x} + v\frac{\partial \zeta}{\partial y} \qquad \text{for } z = \zeta \tag{2.1.6}$$

$$w = -u\frac{\partial H}{\partial x} - v\frac{\partial H}{\partial y} \qquad \text{for } z = -H. \tag{2.1.7}$$

At the bottom boundary, no-slip conditions are prescribed for the horizontal velocity components

$$u = 0 \text{ and } v = 0 \tag{2.1.8}$$

so that with Eq. (2.1.7) $w = 0$ at the bottom. The dynamic boundary conditions at the surface are formulated as

$$(\nu_t + \nu)\frac{\partial u}{\partial z} = \alpha\tau_s^x \tag{2.1.9}$$

$$(\nu_t + \nu)\frac{\partial v}{\partial z} = \alpha\tau_s^y \tag{2.1.10}$$

where τ_s^x and τ_s^y are the surface stresses calculated as a function of meteorological parameters such as wind speed, wind direction and surface roughness. The lateral boundary conditions are chosen such that no flow across material boundaries occurs, i.e. for an eastern or a western closed boundary it follows that $u = 0$. Furthermore, it is assured that the velocity gradients across open boundaries vanish. In the case of an open boundary in the east or west of a model domain, this leads to the consequence that $\partial u/\partial x = \partial v/\partial x = 0$. At so-called forced open boundaries, the sea surface elevation ζ is prescribed while at passive open boundaries the curvature of the surface elevation normal to the boundary is assumed to be zero (i.e. spatial derivatives vanish).

2.1.3 The turbulence model

The turbulent quantities ν_t (eddy viscosity) and ν_t' (eddy diffusivity) are parametrised by means of a turbulence model which uses two parameters, the turbulent kinetic energy (TKE) k and the energy dissipation rate (ERD) ε. An important characteristic of turbulence is the formation of eddies. Eddy

formation occurs at large scales where turbulence is generated via mechanical means (through shear) or via buoyancy. Large eddies are unstable and continuously break down into successively smaller eddies. This phenomenon is often referred to as the turbulent cascade and eddy breakdown occurs in a random or chaotic manner. The flowing liquid possesses mass and velocity and thus has kinetic energy (turbulent kinetic energy). The kinetic energy is passed down through the eddies with some of the energy being used to overcome viscous forces and is thus lost as heat. This loss is described by the energy dissipation rate ε. Eventually, the eddies break down to a size where they have insufficient kinetic energy to form smaller eddies. The smallest eddy size that can be formed is defined by the Kolmogorov length scale. The basic form of the $k-\varepsilon$ model can be written as (*Burchard* [2002])

$$\frac{\partial k}{\partial t} - \frac{\partial}{\partial z}\left(\left(\nu + \frac{\nu_t}{\sigma_k}\right)\frac{\partial k}{\partial z}\right) = P + B - \varepsilon \tag{2.1.11}$$

$$\frac{\partial \varepsilon}{\partial t} - \frac{\partial}{\partial z}\left(\left(\nu + \frac{\nu_t}{\sigma_\varepsilon}\right)\frac{\partial \varepsilon}{\partial z}\right) = \frac{\varepsilon}{k}(c_{1\varepsilon}P + c_{3\varepsilon}B - c_{2\varepsilon}\varepsilon) \tag{2.1.12}$$

with the turbulent kinetic energy equation (2.1.11) and its dissipation rate (2.1.12). The vertical diffusion of k and ε is denoted by the Schmidt numbers σ_k and σ_ε, respectively. P and B are shear and buoyancy production defined as

$$P = \nu_t\left(\left(\frac{\partial u}{z}\right)^2 + \left(\frac{\partial v}{z}\right)^2\right), \qquad B = -\nu_t'\frac{\partial b}{\partial z}. \tag{2.1.13}$$

Empirical parameters in Eq. (2.1.12) are denoted by $c_{1\varepsilon}$, $c_{2\varepsilon}$, and $c_{3\varepsilon}$. Finally, the Kolmogorov-Prandtl expression for eddy viscosity and diffusivity is used

$$\nu_t = c_\mu\frac{k^2}{\varepsilon}, \qquad \nu_t' = c_\mu'\frac{k^2}{\varepsilon} \tag{2.1.14}$$

to calculate ν_t and ν_t' in terms of k and ε. In Eq. (2.1.14) c_μ and c_μ' are so-called stability functions depending on shear, stratification and turbulent time scale, $\tau = k/\varepsilon$.

2.1.4 Transport of tracers

The transport of tracers such as temperature, salinity or chemical substances is already included in GETM by the conservation equation

$$\frac{\partial C^i}{\partial t} + \frac{\partial (uC^i)}{\partial t} + \frac{\partial (vC^i)}{\partial t} + \frac{\partial}{\partial z}\left(\left(w + w_s^i\right) C^i\right) - \frac{\partial}{\partial z}\left(\nu_t' \frac{\partial C^i}{\partial z}\right) - \frac{\partial}{\partial x}\left(A_h^T \frac{\partial C^i}{\partial x}\right) - \frac{\partial}{\partial y}\left(A_h^T \frac{\partial C^i}{\partial y}\right) = Q^i. \tag{2.1.15}$$

Here, C^i represents a number of N_c tracers, so that $1 \leq i \leq N_c$. The terms including the components of the velocity vector estimate the advective transport of the tracer C^i due to the mean flow velocity field. The turbulent diffusive transport of C^i is introduced through the horizontal eddy diffusivity A_h^T and the vertical eddy diffusivity ν_t'. Vertical migration of tracer concentrations such as settling of suspended matter or active migration of micro-organisms is considered by the additional velocity component w_s^i (positive for upward motion). On the right-hand side of Eq. (2.1.15), Q_i denotes all internal sources and sinks of the tracers.

2.1.5 Temporal discretisation: mode splitting

Since the free surface dynamics are included in Eq. (2.1.1) and (2.1.2), the solutions will involve adjustment due to external gravity waves. To avoid numerical instabilities, it is necessary to solve these equations at a time step dictated by the Courant-Friedrichs-Levy (CFL) condition for the fast external gravity waves

$$\Delta t_{ext} < \min\left\{\frac{1}{2}\left(\frac{1}{\Delta x} + \frac{1}{\Delta y}\right)\sqrt{2gD}\right\}^{-1}. \tag{2.1.16}$$

In general, it is computationally too expensive and not necessary to obtain solutions at such high temporal resolution. Thus, it is desirable to eliminate external mode calculations as far as possible. This is achieved by a technique called mode-splitting (*Schwiderski* [1980]) which involves separating out the external (barotropic) and internal (baroclinic) mode equations. Each of them can then be solved separately at appropriate time steps. The external mode uses the depth-integrated momentum equations and the depth-integrated continuity equation to predict water surface elevations and mean horizontal velocities U and V. The baroclinic equations, on the other hand, are solved using a much larger time step dictated by the Courant number

for advection

$$\Delta t_{int} < \min\left\{\frac{\Delta x}{u_{max}}, \frac{\Delta y}{v_{max}}\right\} \tag{2.1.17}$$

where u_{max} and v_{max} are the maximum horizontal advective velocities.
Advection in the internal and external mode of the model is discretised using an explicit numerical scheme for the time differencing while diffusion in the vertical is discretised with an implicit scheme.
In GETM, a macro time step Δt is used for the internal mode while the external mode uses a micro time step Δt_m. The latter is an integer fraction M of the first one and is limited by means of Eq. (2.1.16). The macro time step is limited by the maximum current speed in Eq. (2.1.17). The organisation of the time stepping is shown in Fig. 2.1.1.

2.1.6 Spatial discretisation

The model equations are discretised on an Arakawa-C finite difference grid (*Arakawa and Lamb* [1977]) which belongs to a class of staggered grids. In a C-grid, quantities such as ζ and topographic height H are defined at the centre of the grid while the zonal velocity component u is transposed half a grid to the west of the centre and the meridional component v is displaced half a grid to the south of the centre. The spatial coordinates x and y are located at the corners of each horizontal grid cell and indexing is carried out with i-indices in eastern, j-indices in northern and k-indices in upward direction. Thus, each grid point is defined by a triple (i, j, k). In GETM, the centre of a grid cell is referred to as the tracer point (T-point) because here, all tracers such as temperature T, salinity S, the general tracers C^i and the density ρ are computed. The layout of the horizontal grid is shown in detail in Fig. 2.1.2b. It should be noted that GETM is capable to run on a curvilinear grid. Since all simulations were carried out using a Cartesian rectangular grid with horizontal spatial increments Δx and Δy, this will not be discussed here any further.
For vertical discretisation, the water column is divided into N non-intersecting layers h_k $(k = 1, \cdots, N)$ ranging from the bottom at $z = -H(x, y)$ to the surface at $z = \zeta(x, y, t)$. This is achieved by introducing $N-1$ internal levels z_k $(k = 1, \cdots, N-1)$. The vertical location and the depth $h_k = z_k - z_{k-1}$ of each surface layer depends on the horizontal position (x, y) and time t. All physical quantities are computed on a vertically staggered Arakawa C-grid which consists of control volumes around the T-points. To resolve the surface and bottom boundary layers, the vertical equations of the model are

restructured in a bottom and surface following σ-coordinate system. The σ-coordinate scales the vertical coordinate z by the water depth $D = H + \zeta$, thereby preserving all model layers as the bathymetry and surface elevation change. For σ-coordinates, the internal z-levels can be calculated according to *Freeman et al.* [1972] as

$$z_k = D \underbrace{\frac{k}{N}}_{\sigma_k} - 1 \,. \tag{2.1.18}$$

In σ-coordinates, the surface ($k = N$) is denoted by $\sigma_k = 0$ and for the bottom σ_k becomes -1. The layout of the vertical grid is depicted in Fig. 2.1.2b.

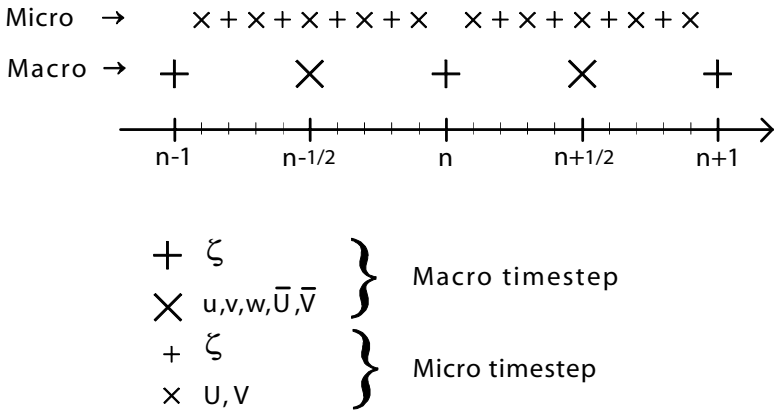

Fig. 2.1.1: Time stepping scheme. u, v, w are the components of the velocity vector and $\bar{U}$, $\bar{V}$ are the time averaged vertical transports calculated only every macro time step. The vertically integrated transports U and V are computed every micro time step. Only the sea surface elevation ζ is determined every micro and macro time step. This figure has been taken from *Burchard and Bolding* [2002].

2.2 The transport equation

In natural waters, transport of tracers is described as a combination of advection and diffusion. Advection is the transport associated with the mean flow of a fluid while diffusion is associated with random motions of molecules and turbulence within a fluid.

2.2.1 The Fickian diffusion equation

Following *Fischer et al.* [1979] it is shown here how to derive the molecular diffusion equation which covers two primary properties: it is random in

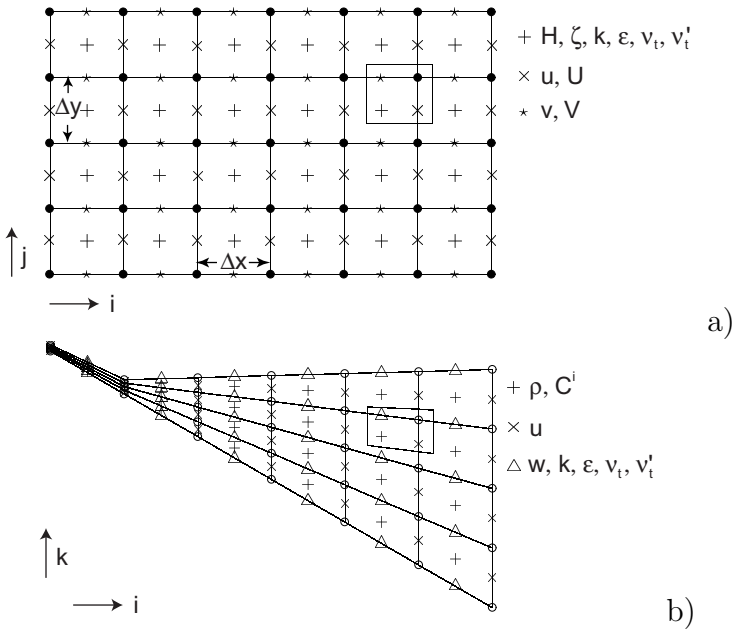

Fig. 2.1.2: a) horizontal model grid and b) vertical grid. Each grid box refers to the tracer point (T-point) in its centre. The physical quantities located on the grid are explained in the text. The following symbols are used: +: T-points; ×: u-points; ⋆: v-points; △: w-points; •: x-points; ○: x^u-points. The inserted frames denote grid points with the same index (i, j) and (i, k), respectively. The figures have been adapted from *Burchard and Bolding* [2002].

nature, and transport is from regions of high concentration to low concentration. To derive a diffusive flux equation, two rows of molecules side-by-side and centred at $x = 0$ are considered (Fig. 2.2.1a). Each of these molecules moves about randomly in response to the temperature. For simplicity's sake only the x-component of their three-dimensional motion is taken into account (i.e. motion to the left or right) with the same constant diffusion velocity for each particle. The mass of molecules on the left is defined as M_l and the mass of molecules on the right as M_r while the probability (transfer rate per time) that one of them moves across $x = 0$ is k. After some time Δt, approximately half of the particles have taken steps to the right and the other half has taken steps to the left as depicted by Fig. 2.2.1b and 2.2.1c. The particle histograms in Fig. 2.2.1 show that maximum concentrations decrease while the total region containing molecules increases (the particle cloud spreads out). Mathematically, the average flux of particles from the left-hand column to the right is $-k\,M_l$ and the average flux of particles from the right-hand column to the left is $-k\,M_r$ where the minus sign is used to distinguish direction. Thus, the net flux q_x is

$$q_x = k\,(M_l - M_r). \tag{2.2.1}$$

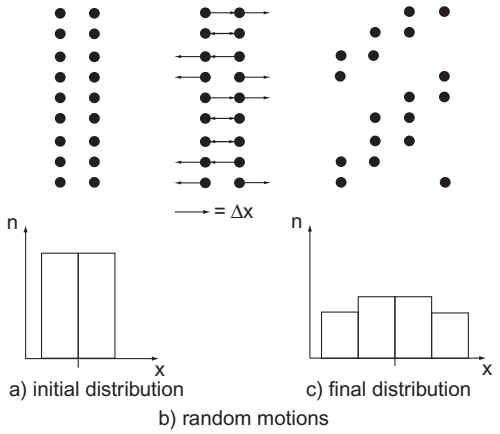

Fig. 2.2.1: Schematic of the one-dimensional molecular (Brownian) motion of a group of molecules illustrating the Fickian diffusion model. The upper part of the figure shows the molecules themselves and the lower part of the figure gives the corresponding histogram of particle location which is analogous to concentration.

Now, Eq. (2.2.1) can be transformed into an equation for C by considering that for the one-dimensional case concentration is mass M per length $\Delta x = x_r - x_l$

$$C_l = \frac{M_l}{\Delta x} \tag{2.2.2}$$

$$C_r = \frac{M_r}{\Delta x} \tag{2.2.3}$$

and by noting that $\frac{dC}{dx}$ is defined as

$$\frac{dC}{dx} = \frac{C_r - C_l}{x_r - x_l} = \frac{C_r - C_l}{\Delta x}. \tag{2.2.4}$$

Let now Δx be the length of the average step in x-direction taken by a particle in the time Δt. Combining Eq. (2.2.2) with Eq. (2.2.4) gives

$$\frac{dC}{dx} = \frac{M_r - M_l}{(\Delta x)^2} \Leftrightarrow M_l - M_r = -(\Delta x)^2 \frac{dC}{dx}, \tag{2.2.5}$$

which can be substituted into Eq. (2.2.1) to yield

$$q_x = -k\,(\Delta x)^2 \frac{dC}{dx} = -D \frac{dC}{dx} \tag{2.2.6}$$

where D represents the molecular diffusion coefficient. The molecular diffusion coefficient is a molecular property and not a characteristic of the flow. Generalising to three dimensions, the diffusive flux vector $\vec{q}$ can be found by adding the other two dimensions (y and z), yielding

$$\begin{aligned} \vec{q} &= -D \left(\frac{\partial C}{\partial x}, \frac{\partial C}{\partial y}, \frac{\partial C}{\partial z} \right) \\ &= -D \nabla C. \end{aligned} \tag{2.2.7}$$

Diffusion processes that obey this relationship are called Fickian processes, and Eq. (2.2.7) is called Fick's law. The diffusive flux $\vec{q}$ is expressed in units kg/(m^2 s). In order to compute a total mass flux rate m with units kg/s the normal component of the diffusive flux vector has to be integrated over a surface area A

$$m = \iint_A \vec{q} \cdot \vec{n} \, dA \tag{2.2.8}$$

where $\vec{n}$ is the unit vector normal to the surface element dA. Although Fick's law gives an expression for the flux of mass due to diffusion, an equation that predicts the change in concentration of the diffusing mass over time at a point (i.e. $\frac{\partial C}{\partial t}$) is still needed. Such an equation can be derived by determining the change in concentration with time C of a dissolved substance in a fixed control volume CV (i.e. $\Delta x, \Delta y, \Delta z = \Delta V = const.$) together with the law of conservation of mass as depicted in Fig. 2.2.2

$$\frac{\partial}{\partial t} \iiint_V C \, dV. \tag{2.2.9}$$

It should be noted that a change in C only occurs due to mass flux through the surface areas (i.e. no sources or sinks are present in CV). For the x-direction the net flux q_x according to Fick's law is

$$q_x = q_{x,in} - q_{x,out} \quad = \quad -D \left(\left. \frac{\partial C}{\partial x} \right|_{x=1} - \left. \frac{\partial C}{\partial x} \right|_{x=2} \right). \tag{2.2.10}$$

Here, $x = 1$ and $x = 2$ are the locations of the left and right surface areas of CV in x-direction, respectively. The net mass flux rate m for CV is Eq. (2.2.8) and conservation of mass requires that

$$\frac{\partial}{\partial t} \iiint_V C dV + \iint_A \vec{q} \cdot \vec{n} \, dA = 0. \tag{2.2.11}$$

By bringing the time differentiation inside the volume integral and applying the divergence theorem of Gauss

$$\iiint_V \nabla \cdot \vec{q} \, dV = \iint_A \vec{q} \cdot \vec{n} \, dA \tag{2.2.12}$$

to the surface integral, Eq. (2.2.11) can be written as

$$\iiint_V \left(\frac{\partial C}{\partial t} + \nabla \cdot \vec{q} \right) \, dV = 0. \tag{2.2.13}$$

Since this equation holds for an arbitrary volume CV, the integrand must vanish thus leading to

$$\frac{\partial C}{\partial t} + \nabla \cdot \vec{q} = 0. \tag{2.2.14}$$

Substituting Eq. (2.2.7) into Eq. (2.2.14) yields the molecular diffusion equation

$$\frac{\partial C}{\partial t} = D\Delta C \tag{2.2.15}$$

or fully written out in Cartesian coordinates

$$\frac{\partial C}{\partial t} = D\left(\frac{\partial^2 C}{\partial x^2} + \frac{\partial^2 C}{\partial y^2} + \frac{\partial^2 C}{\partial z^2}\right). \tag{2.2.16}$$

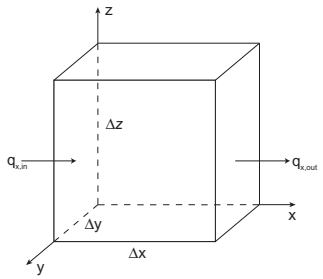

Fig. 2.2.2: Differential control volume CV for derivation of the diffusion equation.

2.2.2 The advection-diffusion equation

The derivation of the advection-diffusion equation relies on the principle of superposition: advection and diffusion can be added together because they are linearly independent of each other (i.e. one process does not feed back on the other). Due to diffusion, each particle moves in time Δt either one step to the left or one step to the right (i.e. Δx). Due to advection, each particle will also move $u\Delta t$ in x-direction. The net movement of the particle is $u\Delta t \pm \Delta x$ and thus, the total flux for three-dimensional flow $\vec{J}$, including the advective transport and a Fickian diffusion term, must be

$$\vec{J} = \vec{u}C + \vec{q} = \vec{u}C - D\nabla C \tag{2.2.17}$$

where $\vec{u} = (u, v, w)$ is the velocity vector. This flux law and conservation of mass can be used to derive the advection-diffusion equation. To do this, the control volume CV is used again with a cross sectional flow as depicted by Fig. 2.2.3. The net mass flux rate m for CV is

$$m = \iint_A \vec{J} \cdot \vec{n}\, dA. \tag{2.2.18}$$

Substituting Eq. (2.2.18) into Eq. (2.2.11) and following the reasoning which has lead to Eq. (2.2.14) yields

$$\frac{\partial C}{\partial t} + \nabla \cdot \vec{J} = 0. \tag{2.2.19}$$

Replacing $\vec{J}$ with Eq. (2.2.17) gives the advection-diffusion equation as

$$\frac{\partial C}{\partial t} + \nabla \cdot (\vec{u}\, C) = D\ \Delta C \tag{2.2.20}$$

The equation of continuity for incompressible flow is $\nabla \cdot \vec{u} = 0$ and Eq. (2.2.20) becomes

$$\frac{\partial C}{\partial t} + \vec{u} \cdot \nabla C = D\ \Delta C. \tag{2.2.21}$$

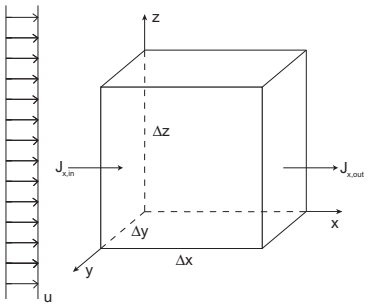

Fig. 2.2.3: Schematic of a control volume CV with cross flow.

2.2.3 Turbulent diffusion

Molecular diffusion alone is entirely insufficient to produce the rate of mixing observed in natural waters. The difference between the observed rate of diffusion and the rate expected from molecular diffusion is the result of turbulent diffusion. Thus, the advection-diffusion equation has to be extended to include the influence of turbulence. A conservation equation for turbulent flows can be derived from the advection-diffusion equation by decomposing the velocity vector and the concentration into the sum of a time averaged and a fluctuating part

$$C = \overline{C} + C', \tag{2.2.22}$$

$$u = \overline{u} + u', \tag{2.2.23}$$

$$v = \overline{v} + v', \tag{2.2.24}$$

$$w = \overline{w} + w' \tag{2.2.25}$$

where $^-$ denotes the time average and $'$ is the instantaneous fluctuation (or deviation from the mean). The following rules for time averaging of Eq. (2.2.22) - (2.2.25) are assumed (see *Burchard* [2002])
1. Time average of the time average:

$$\overline{\overline{\Psi}} = \overline{\Psi} \tag{2.2.26}$$

2. Time average of the fluctuation:

$$\overline{\Psi'} = 0 \tag{2.2.27}$$

3. Linearity:

$$\overline{\Psi + \lambda\,\Psi} = \overline{\Psi} + \lambda\overline{\Psi} \tag{2.2.28}$$

4. Product average:

$$\overline{\overline{\Psi}\overline{\Psi}} = \overline{\Psi}\overline{\Psi} \tag{2.2.29}$$

$$\overline{\overline{\Psi}\Psi'} = 0 \tag{2.2.30}$$

$$\overline{\Psi'\Psi'} \neq 0 \tag{2.2.31}$$

5. Derivatives and average commute:

$$\overline{\frac{\partial\Psi}{\partial x}} = \frac{\partial\overline{\Psi}}{\partial x} \tag{2.2.32}$$

Substituting Eq. (2.2.22) - (2.2.25) into Eq. (2.2.20) gives

$$\begin{aligned}
\frac{\partial(\overline{C}+C')}{\partial t} &+ (\overline{u}+u')\,\frac{\partial(\overline{C}+C')}{\partial x} + (\overline{v}+v')\,\frac{\partial(\overline{C}+C')}{\partial y} \\
&+ (\overline{w}+w')\,\frac{\partial(\overline{C}+C')}{\partial z} + (\overline{C}+C')\frac{\partial\overline{u}+u'}{\partial x} \\
&+ (\overline{C}+C')\,\frac{\partial(\overline{v}+v')}{\partial y} + (\overline{C}+C')\frac{\partial\overline{w}+w'}{\partial z} \\
&= D\frac{\partial^2\overline{C}+C'}{\partial x^2} + D\frac{\partial^2\overline{C}+C'}{\partial y^2} + D\frac{\partial^2\overline{C}+C'}{\partial z^2}
\end{aligned} \tag{2.2.33}$$

Time averaging of Eq. (2.2.33) with respect to the rules (2.2.26) - (2.2.32) yields

$$\frac{\partial\overline{C}}{\partial t} + \nabla\cdot(\overline{\vec{u}}\,\overline{C}) = D\Delta\overline{C} - \frac{\partial}{\partial x}(\overline{u'C'}) - \frac{\partial}{\partial y}(\overline{v'C'}) - \frac{\partial}{\partial z}(\overline{w'C'}). \tag{2.2.34}$$

The time averaged transport equation (2.2.34) is similar to the instantaneous equation (2.2.20) with the addition of the last three terms on the right-hand

side which correspond to the transport of C by turbulent fluctuations. These additional terms can be rewritten together with the diffusive transport $D\Delta\overline{C}$ as

$$\frac{\partial}{\partial x}\left(D\frac{\partial\overline{C}}{\partial x}-\overline{u'C'}\right)+\frac{\partial}{\partial y}\left(D\frac{\partial\overline{C}}{\partial y}-\overline{v'C'}\right)+\frac{\partial}{\partial z}\left(D\frac{\partial\overline{C}}{\partial z}-\overline{w'C'}\right). \quad (2.2.35)$$

All terms in the parentheses represent mass transport. The first of these terms stands for the transport due to molecular diffusion (Fick's law) and the second is a turbulent flux that arises by virtue of the correlation between $\vec{u'}$ and C' where $\vec{u'}=(u',v',w')$. Since the molecular diffusion coefficient is usually a very small quantity (i.e. $\overline{\vec{u'}C'} \gg D\frac{\partial C}{\partial x}$), the molecular diffusion terms can be neglected compared to turbulent flux. The terms denoting the turbulent transport represent unknown quantities. Assuming that the turbulent diffusion is a Fickian process, this closure problem is solved by introducing a coefficient of eddy diffusivity for each direction. With this assumption and the notation A_x, A_y for the horizontal eddy diffusivities and ν' for the vertical eddy diffusivity, the closure scheme is

$$\overline{u'C'}=-A_x\frac{\partial C}{\partial x} \qquad \overline{v'C'}=-A_y\frac{\partial C}{\partial y} \qquad \overline{w'C'}=-\nu'\frac{\partial C}{\partial z}. \quad (2.2.36)$$

The coefficients A_x, A_y, ν' are strongly flow dependent and vary within the flow field. With the assumption that turbulent mixing is much stronger than molecular diffusion the transport equation for turbulent flow is

$$\frac{\partial C}{\partial t}+\nabla\cdot(\vec{u}\,C)=\frac{\partial}{\partial x}\left(A_x\frac{\partial C}{\partial x}\right)+\frac{\partial}{\partial y}\left(A_y\frac{\partial C}{\partial y}\right)+\frac{\partial}{\partial z}\left(\nu'\frac{\partial C}{\partial z}\right). \quad (2.2.37)$$

2.2.4 Eulerian vs. Lagrangian perspective

Fluid motion and any constituent (temperature, salinity, concentration of an arbitrary substance) transported by fluid motion can be described from two frames of reference, from a stationary frame (Eulerian) and from one which is moving along with the flow (Lagrangian). In the Eulerian perspective, the flow and its constituents are described with respect to fixed spatial positions $\vec{x}=(x,y,z)$ and time t. Thus, they are written as e.g. $\vec{u}(\vec{x},t)$ and $C(\vec{x},t)$. The Lagrangian perspective follows the flow and traces the history of individual fluid particles. Unlike in the Eulerian description, spatial position is not a fixed reference but another variable of the particle. The flow variables are written with respect to time t and to a single, initial reference position, e.g. $\vec{x}_0$ the particle position at $t=0$. In this case all variables are recorded as e.g. $\vec{x}(\vec{x}_0,t)$ and $C(\vec{x}_0,t)$.

Now, let us assume that any flow variable in fixed Eulerian coordinates is represented by $\Psi(x, y, z, t)$. A change in Ψ due to a small change in spatial position $d\vec{x} = (dx, dy, dz)$ and time dt can be written as

$$d\Psi = \frac{\partial \Psi}{\partial t}dt + \frac{\partial \Psi}{\partial x}dx + \frac{\partial \Psi}{\partial y}dy + \frac{\partial \Psi}{\partial z}dz. \tag{2.2.38}$$

In order to obtain the rate of change of Ψ while following the trajectory of an individual particle through the flow (Lagrangian perspective), Eq. (2.2.38) is divided by dt which leads to

$$\begin{aligned} \frac{d\Psi}{dt} &= \frac{\partial \Psi}{\partial t} + \frac{\partial \Psi}{\partial x}\frac{dx}{dt} + \frac{\partial \Psi}{\partial y}\frac{dy}{dt} + \frac{\partial \Psi}{\partial z}\frac{dz}{dt} \\ &= \frac{\partial \Psi}{\partial t} + u\frac{\partial \Psi}{\partial x} + v\frac{\partial \Psi}{\partial y} + w\frac{\partial \Psi}{\partial z}\frac{dz}{dt} \\ &= \frac{\partial \Psi}{\partial t} + \vec{u} \cdot \nabla \Psi \end{aligned} \tag{2.2.39}$$

where d/dt denotes the total (or substantial) derivative. Thus, the advection-diffusion equation can be written in two ways. The Eulerian form was already shown in the last section to be (see Eq. (2.2.37)

$$\frac{\partial C}{\partial t} + \nabla \cdot (\vec{u}\, C) = \frac{\partial}{\partial x}\left(A_x \frac{\partial C}{\partial x}\right) + \frac{\partial}{\partial y}\left(A_y \frac{\partial C}{\partial y}\right) + \frac{\partial}{\partial z}\left(\nu' \frac{\partial C}{\partial z}\right). \tag{2.2.40}$$

The Lagrangian advection-diffusion equation can be obtained by substituting Eq. (2.2.39) into Eq. (2.2.40)

$$\frac{dC}{dt} + C\nabla \cdot \vec{u} = \frac{\partial}{\partial x}\left(A_x \frac{\partial C}{\partial x}\right) + \frac{\partial}{\partial y}\left(A_y \frac{\partial C}{\partial y}\right) + \frac{\partial}{\partial z}\left(\nu' \frac{\partial C}{\partial z}\right). \tag{2.2.41}$$

2.3 Modelling transport

Modelling transport in fluids of any arbitrary substance can be done in several ways. As proposed by the advection-diffusion equation, one could compute the change in concentration of a substance at a number of points in the fluid volume. If this is done with respect to the Eulerian view, concentration C is calculated on grid points which are fixed in space. On the other side, if one is interested in the change of C while moving with the flow (Lagrangian perspective), the grid points on which C is evaluated must follow the flow (*Maier-Reimer* [1973]), i.e. the grid is deformed with time (Lagrangian grid). In his study, *Maier-Reimer* [1973] successfully adapted the "TUrbulent Diffusion in LAGrangian coordinates"-scheme (TUDLAG) and a mixed scheme where C is transformed from the Lagrangian to an

Eulerian grid (TUDELM) to model transport in the North Sea. A major disadvantage of this method is the progressive deformation of the grid which in extreme cases leads to numerical instability (e.g. a two-dimensional grid cell degenerates to a straight line). Another approach by *Maier-Reimer and Sündermann* [1982] proposed to interpret the water body not as a continuum but as finite set of water particles with fixed physical properties (tracer method). The physical state of an Eulerian variable on the grid points is defined as the mean value of all particles situated in a grid cell. This approach can be generalised to include all physical properties such as velocity, density, temperature and dissolved substances. In the case of a dissolved substance, it is represented by a discrete number of tracer particles which is proportional to the concentration C in the grid cell. Instead of modelling advection and diffusion in terms of concentration, the motions of the tracer particles due to the mean current field and turbulent velocity fluctuations and hereby their paths (trajectories) are calculated. Compared to the established finite techniques, tracer methods have the great profit of almost completely avoiding unwanted numerical diffusion and thereby assure more accurate results. *Maier-Reimer* [1973] pointed out the criteria a numerical method for the advection-diffusion equation has to satisfy in order to reproduce the dynamics of the physical property which is transported:

1. Positivity: this criterion ensures that positive properties stay positive.

2. Conservation of local mass: in absence of external sources and sinks, the total quantity of a property must be constant with time

$$\frac{\partial}{\partial t}\iiint_V C(x,y,z,t)\; dxdydz = 0. \tag{2.3.1}$$

3. No numerical diffusion: in the case where turbulent diffusion is absent, the numerical method must describe transport as it occurs solely due to advection.

In general, it is difficult to satisfy all three criteria with a numerical scheme in Eulerian coordinates. See, however, *Pietrzak* [1998] for a method of incorporating monotone high-order advection schemes with low numerical diffusion in three-dimensional models. This method has also been applied by *Burchard and Bolding* [2002] for GETM. Nevertheless, particle methods have benefits which can be summarised (*Dimou and Adams* [1993]) as follows:

1. Sources are more easily represented in a particle tracking model, whereas concentration models have difficulty resolving concentration fields whose spatial extent is small compared to that of discretisation.

2. In particle tracking models the computational effort is concentrated in regions where most particles are located, while in concentration models all regions of the domain are treated equally in terms of computational effort.

3. The parallel nature of tracer models is better suited to the capabilities of parallel computing.

4. In the Eulerian frame it becomes difficult to model sharp gradients (i.e. brackish zones), since numerical diffusion is likely to be high near extremes in tracer concentration so that results tend to be unrealistic. Using tracer methods there is almost no numerical diffusion.

5. Particle tracking models are more natural where transport and fate processes are best described by attributes of the individual particles (e.g. settling of different size particles) rather than their aggregation (i.e. concentration).

6. Particle tracking models are a direct choice if an integrated property of the concentration distribution (i.e. residence time) and not the concentration distribution itself is concerned.

Particle methods have been used in coastal applications to display residual circulation (*Signell and Geyer* [1990]) and in concentration-based models for predicting and displaying pollutant concentrations (*Duwe et al.* [1987], *Müller-Navarra and Mittelstaedt* [1987], *Dick and Soetje* [1990]). Furthermore, a Lagrangian dispersion model was implemented by *Dick and Schönfeld* [1996] to determine water transport, water exchange and mixing times in sub-areas of the North Frisian Wadden Sea.

2.4 Modelling Lagrangian tracers

The transport model describes the motion of a number of discrete particles whose positions vary due to advection and turbulence. To do this, transport is divided into an advective and a diffusive component and each of them is modelled separately. The advection equation is solved analytically while turbulent diffusion is modelled with a random walk scheme. In the following sections, the analytical solution of the advection equation is derived and a brief description of the stochastic theory behind the random walk model is given. Furthermore, details on the implementation of the algorithms are given.

2.4.1 Modelling advection

The movement of a Lagrangian tracer due to advection is described by the ordinary differential equation

$$\frac{d\vec{x}_T}{dt} = \vec{v}_T(\vec{x}_T(t)) \tag{2.4.1}$$

where $\vec{x}_T(t) = (x_T(t), y_T(t), z_T(t))$ is the particle position and $\vec{v}_T(\vec{x}_T(t)) = (u_T(\vec{x}_T(t)), v_T(\vec{x}_T(t)), w_T(\vec{x}_T(t))$ is the corresponding velocity vector. To calculate the movement of particles one can either apply a standard numerical integration scheme to the equation of motion (2.4.1) (e.g. the Runge-Kutta method) or find its analytical solution. The analytical solution is not difficult to obtain and has the advantage that the results based on it are very accurate.

2.4.1.1 Interpolation scheme

An interpolation scheme is necessary to transform the velocity components calculated by GETM from the Eulerian grid to the position $\vec{x}_T$ of a tracer. *Maier-Reimer* [1973] used bilinear interpolation on an Arakawa C-grid considering four points for each velocity component. As two of these four points are always located outside the grid box containing the tracer particle, they are inappropriate to reflect the flow within this grid cell. Furthermore in GETM, the discretised equation of continuity only takes into account the velocity points defined on the boundaries of each grid box to guarantee conservation of mass. Thus, applying bilinear interpolation would clearly violate the equation of continuity. The linear interpolation applied by *Duwe* [1988] only uses the six velocity points defined on the boundaries of each grid box and thus conserves mass. As a consequence the velocity components within a grid box are solely functions of their corresponding direction (i.e. $\partial u/\partial y = \partial u/\partial z = 0$). This has two advantages:

1. the interpolation scheme and hence the Lagrangian tracer model is consistent with GETM (mass conserving) which computes the velocity and

2. the acceleration of a particle on its path is easily calculated.

To determine the velocity at the location of a particle in the grid box denoted by (i, j, k) the following linear equations are used

$$u_T(\vec{x}) = a \cdot u(i,j,k) + (1-a) \cdot u(i-1,j,k) \tag{2.4.2}$$

$$v_T(\vec{x}) = b \cdot v(i,j,k) + (1-b) \cdot v(i,j-1,k) \tag{2.4.3}$$

$$w_T(\vec{x}) = c \cdot w(i,j,k) + (1-c) \cdot w(i,j,k-1) \tag{2.4.4}$$

where a, b and c are the weighting factors (Fig. 2.4.1)

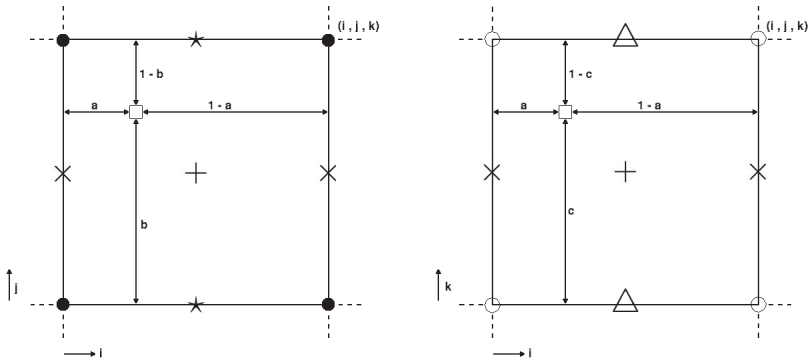

Fig. 2.4.1: Shown is the reference box for the tracer position with the weighting factors a, b, c used to linearly interpolate u, v and w. The following symbols are used: $\square$: tracer position $+$: T-points; $\times$: u-points; $\star$: v-points; $\triangle$: w-points; $\bullet$: x-points; $\circ$: x^u-points.

2.4.1.2 Analytical solution of the advection equation

Following *Schönfeld* [1994] it is shown here how to derive the analytical solution for the one-dimensional equation of particle movement. Equation (2.4.1) can be written as the linear interpolation from the already known velocity field as follows

$$\frac{dx_T}{dt} = u_T = \frac{x_T - x_l}{x_r - x_l} u_r + \left[1 - \frac{x_T - x_l}{x_r - x_l}\right] u_l. \tag{2.4.5}$$

Here x_l, x_r are fixed grid points, x_T is the position of a particle in between and u_l, u_r are the velocities at x_l and x_r, respectively. This linear inhomogeneous first order ordinary differential equation can be solved by means of the integrating factor technique. As a first step towards the solution Eq. (2.4.5) is rewritten as

$$\frac{d\vec{x}_T}{dt} + x_T \cdot \underbrace{-\frac{\Delta u}{\Delta x}}_{=f(t)} = u_l - x_l \frac{\Delta u}{\Delta x} \tag{2.4.6}$$

where $\Delta u = u_r - u_l$ and $\Delta x = x_r - x_l$. In a next step the antiderivative $F(t) = -t\frac{\Delta u}{\Delta x}$ to $f(t)$ is found and the integration factor $e^{F(t)}$ is formed. Then, Eq. (2.4.6) is multiplied with the integration factor which yields

$$\frac{d}{dt}\left(x_T\, e^{-t\frac{\Delta u}{\Delta x}}\right) = e^{-t\frac{\Delta u}{\Delta x}}\left(u_l - x_l\frac{\Delta u}{\Delta x}\right). \tag{2.4.7}$$

Integration of both sides with respect to t gives

$$x_T\,(t) = x_l - u_l\frac{\Delta x}{\Delta u} + Ce^{t\frac{\Delta u}{\Delta x}} \tag{2.4.8}$$

where C is the integration constant. C can be determined through the initial condition $x_T(t_0) = x_{T,0}$ (i.e. initial position of the particle)

$$x_T(t_0) = x_{T,0} = x_l - u_l\frac{\Delta x}{\Delta u} + Ce^{t_0\frac{\Delta u}{\Delta x}}$$

$$\Leftrightarrow C = \left(x_{T,0} + u_l\frac{\Delta x}{\Delta u} - x_l\right)e^{-t_0\frac{\Delta u}{\Delta x}} \tag{2.4.9}$$

As a final step $x_{T,0}$ is replaced in Eq. (2.4.9) by recognising

$$\left.\frac{dx}{dt}\right|_{t=t_0} = u_{T,0} = x_{T,0}\frac{\Delta u}{\Delta x} + u_l - x_l\frac{\Delta u}{\Delta x}$$

$$\Leftrightarrow x_{T,0} = u_{T,0}\frac{\Delta x}{\Delta u} + x_l - u_l\frac{\Delta x}{\Delta u} \tag{2.4.10}$$

such that the particle position can be readily determined as

$$x_T(t) = u_{T,0}\frac{\Delta x}{\Delta u}e^{\frac{\Delta u}{\Delta x}(t-t_0)}. \tag{2.4.11}$$

The distance $\Delta x_T = x_T\,(t) - x_{T,0}$ a particle travels during a time step $\Delta t = t - t_0$ is then

$$\Delta x_T = \frac{u_{T,0}\,\Delta x}{\Delta u}\left(e^{\frac{\Delta t\,\Delta u}{\Delta x}} - 1\right) \tag{2.4.12}$$

In Appendix B a second way to obtain the solution to the movement equation (2.4.12) is presented. In analogy to Eq. (2.4.12) the movement of a particle in x and y-direction is

$$\Delta y_T = \frac{v_{T,0}\,dy}{\Delta v}\left(e^{\frac{\Delta t\,\Delta v}{dy}} - 1\right) \tag{2.4.13}$$

$$\Delta z_T = \frac{w_{T,0}\,\Delta z}{\Delta w}\left(e^{\frac{\Delta t\,\Delta w}{\Delta z}} - 1\right). \tag{2.4.14}$$

For uniform flow (i.e., $\Delta u = \Delta v = \Delta w = 0$) the particle motion is simply calculated with

$$\Delta x_T = u_{T,0}\,\Delta t \tag{2.4.15}$$

$$\Delta y_T = v_{T,0}\,\Delta t \tag{2.4.16}$$

$$\Delta z_T = w_{T,0}\,\Delta t. \tag{2.4.17}$$

2.4.1.3 Interpolation between grid cells

The interpolation scheme (2.4.2) - (2.4.4) is only valid for the reference box for the current particle position. Thus, if the tracer crosses the boundary to any adjacent cell within a given time step, interpolation has to be carried out again considering the velocity points valid for the new cell. This can be achieved by computing the time necessary for a particle to reach one of the surrounding boundaries $x_{\text{boundary}}, y_{\text{boundary}}$ and z_{boundary}. Which of the two boundaries in a certain direction can be reached is determined by the algebraic sign of the corresponding velocity component at the position of a particle (i.e. if $u > 0$ then the boundary at index i can be reached and if $u < 0$ then the boundary at index $i - 1$ can be reached). The time $\Delta t_x, \Delta t_y, \Delta t_z$ a tracer particle needs to travel the distance

$$\Delta x_T = x_{\text{boundary}} - x_T$$
$$\Delta y_T = y_{\text{boundary}} - y_T$$
$$\Delta z_T = z_{\text{boundary}} - z_T$$

to a boundary is calculated by rewriting Eq. (2.4.12) - (2.4.14) with respect to Δt

$$\Delta t_x = \ln\left(\frac{\Delta x_T\ \Delta u}{\Delta x\ u_T} + 1\right)\frac{\Delta x}{\Delta u} \tag{2.4.18}$$
$$\Delta t_y = \ln\left(\frac{\Delta y_T\ \Delta v}{\Delta y\ v_T} + 1\right)\frac{\Delta y}{\Delta v} \tag{2.4.19}$$
$$\Delta t_z = \ln\left(\frac{\Delta z_T\ \Delta w}{\Delta z\ w_T} + 1\right)\frac{\Delta z}{\Delta w}. \tag{2.4.20}$$

The advection step is then carried out with a time step

$$\Delta t_T = \min(\Delta t_x, \Delta t_y, \Delta t_z, \Delta t) \tag{2.4.21}$$

where Δt is the macro time step for the internal mode of GETM. A particle reaches a boundary, if $\Delta t_T \leq \Delta t$ and it continues its path in the next cell with the new interpolated velocity and the remaining time. If another boundary is crossed, the same procedure applies.

2.4.1.4 Implementation

The Lagrangian advection scheme has been implemented under consideration of the properties mentioned in the last sections. For reasons of simplicity, all calculations have been carried out with respect to spatial coordinates

i, j, k and not x,y,z. The position of a particle as well as its velocity is transformed by dividing their components by the corresponding grid spacing (i.e. $\vec{x}_T = (x_T/\Delta x, y_T/\Delta y, z_T/\Delta z) = (i_T, j_T, k_T)$. The index (i, j, k) of the grid box containing a particle is computed from the particle position as

$$i = \text{int}(i_T + 0.5) \tag{2.4.22}$$
$$j = \text{int}(j_T + 0.5) \tag{2.4.23}$$
$$k = \text{int}(k_T + 0.5). \tag{2.4.24}$$

Necessary for the interpolation of the velocity are the weighting factors which are determined through

$$a = i_T - \text{real}(i - 1) \tag{2.4.25}$$
$$b = j_T - \text{real}(j - 1) \tag{2.4.26}$$
$$c = k_T - \text{real}(k - 1) \tag{2.4.27}$$

so that the tracer velocity can be obtained from Eq. (2.4.2) - (2.4.4). Finally, the position is updated with respect to crossing of boundaries

$$i_T^{n+1} = i_T^n + \frac{u_T^n}{\Delta u}\left(e^{\Delta t_T\, \Delta u} - 1\right) \tag{2.4.28}$$
$$j_T^{n+1} = j_T^n + \frac{v_T^n}{\Delta v}\left(e^{\Delta t_T\, \Delta v} - 1\right) \tag{2.4.29}$$
$$k_T^{n+1} = k_T^n + \frac{w_T^n}{\Delta w}\left(e^{\Delta t_T\, \Delta w} - 1\right). \tag{2.4.30}$$

The gradients of u, v and w are discretised as

$$\Delta u = \frac{u^{n+\frac{1}{2}}(i, j, k) - u^{n+\frac{1}{2}}(i - 1, j, k)}{\Delta x} \tag{2.4.31}$$
$$\Delta v = \frac{v^{n+\frac{1}{2}}(i, j, k) - v^{n+\frac{1}{2}}(i, j - 1, k)}{\Delta y} \tag{2.4.32}$$
$$\Delta w = \frac{w^{n+\frac{1}{2}}(i, j, k) - w^{n+\frac{1}{2}}(i, j, k - 1)}{h(i, j, k)}, \tag{2.4.33}$$

since they are updated in GETM with an offset of $1/2\Delta t$ (see Fig. 2.1.1).

2.4.2 Modelling diffusion

2.4.2.1 The stochastic differential equation (SDE)

In 1908, Langevin considered the problem of the dynamical description of molecular diffusion. He suggested that the equation of motion of a particle

can be described by the following differential equation for the velocity $\vec{v}$

$$\frac{d\vec{v}}{dt} = -\gamma\vec{v} + \vec{L}(t), \tag{2.4.34}$$

where the terms on the right-hand side model the forces which act on the particle. The first term is the dissipative drag force proportional to the particle velocity and γ denotes the friction coefficient. The second term incorporates irregular changes in the velocity caused by random collisions with other particles. The external force $\vec{L}(t)$ is a vector consisting of zero mean, temporally uncorrelated random components $\xi(t)$. They can be described as a stochastic process with mean $\langle\xi(t)\rangle = 0$ and statistical independence defined as $\langle\xi(t+\Delta t)\xi(t)\rangle = \delta(\Delta t)$ for $\Delta t \neq 0$. Here, $\delta(\Delta t)$ is Dirac's delta function with the following property

$$\lim_{\Delta t\to 0} \delta(\Delta t) = \infty$$

which satisfies the requirement of non-correlation at different times. From statistical independence, it follows that $\xi(t)$ has unlimited variance $\big\langle(\xi(t) - \underbrace{\langle\xi(t)\rangle}_{=0})^2\big\rangle = \langle\xi(t)^2\rangle$. A stochastic process $\xi(t)$ with the properties above is called Gaussian white noise.

The Langevin equation is the prototype of a stochastic differential equation (SDE), i.e. a differential equation with a random term which has some given statistical properties. This concept can be used in particle tracking models to describe the position $\vec{x}(t) = (x(t), y(t), z(t))$ of each tracer as (see *Gardiner* [1983])

$$\frac{d\vec{x}(t)}{dt} = \vec{A}(\vec{x}, t) + \mathbf{B}(\vec{x}, t)\vec{L}(t) \tag{2.4.35}$$

where $\vec{A}(\vec{x}, t)$ is a known vector representing the deterministic forces which act to change $\vec{x(t)}$ (e.g. transport by the mean velocity field). The second term consists of a known tensor $\mathbf{B}$ that characterises the random forces (e.g. turbulence) and a vector $\vec{L}(t)$ whose components are random numbers $\xi(t)$ representing the random and chaotic nature of e.g. turbulent diffusion. Here, $\xi(t)$ is a Gaussian white noise process with the already mentioned properties. The solution to this random differential equation is problematic because the presence of randomness prevents the system from having bounded measure and the derivative does not exist. One way to deal with equations such as Eq. (2.4.35) is to write them in differential form

$$d\vec{x}(t) = \vec{A}(\vec{x}, t)dt + \mathbf{B}(\vec{x}, t)\vec{\xi}(t)dt \tag{2.4.36}$$

where dt denotes an infinitesimal step Δt and $\vec{\xi}(t)dt$ is defined as an increment of the Wiener process $\vec{W}(t)$. This random process was named after the American mathematician Norbert Wiener who studied the phenomenon of Brownian motion and gave its mathematical design. The Wiener process $W(t)$ describes the path of a particle due to Brownian motion with time t and consists of an accumulation of independently distributed stochastic increments $dW(t)$. If $W(t)$ and $W(t+dt)$ are the values of the function at times t and $t+dt$, respectively, then $dW(t)$ stands for the increment of the process in the infinitesimal interval dt

$$dW(t) = W(t+dt) - W(t) = \xi(t)\, dt. \tag{2.4.37}$$

Furthermore, $W(t)$ has the following properties (see *Gardiner* [1983]):

1. Start: $W(t=0) \equiv 0$ (unless a different starting point is specified),
2. Trajectories: paths (trajectories) are continuous functions of $t \in [0, \infty)$,
3. Mean: $\langle W(t) \rangle \equiv 0$,
4. Correlation function: $\langle W(t)\, W(s) \rangle = \min(a, b)$,
5. Gaussian distribution: for any $t_1, \cdots, t_n$ the random vector $(W(t_1), \cdots, W(t_n))$ is Gaussian,
6. For any s,t: a) $\langle W(t)^2 \rangle \equiv t$,
   b) $\langle W(t) - W(s) \rangle \equiv 0$,
   c) $\langle (W(t) - W(s))^2 \rangle = \langle W(t)^2 \rangle + \langle W(s)^2 \rangle - 2 \langle W(t)\, W(s) \rangle$
   $= t + s - 2\min(t, s) = \left\{ \begin{array}{ll} t-s & t > s \\ 0 & t = s \\ s-t & t < s \end{array} \right\} = \big|t - s\big|,$
7. Variance: $\langle (W(t) - \langle W(t) \rangle)^2 \rangle = \langle W(t)^2 \rangle = t$,
8. Increment: from property 5 and 6 b), c) it follows that

   $$dW(t) = W(s) - W(t+dt) \ \in \mathcal{N}(0, \sqrt{dt}) \tag{2.4.38}$$

   where $\mathcal{N}(0, \sqrt{dt})$ is a set of Gaussian random numbers with zero mean and a standard deviation of $\sqrt{dt}$,
9. Increment: all increments $W(t_2) - W(t_1), \cdots, W(t_n) - W(t_{n-1})$ are statistically independent of each other for $t_1 \leq t_2 \leq \cdots \leq t_{n-1} \leq t_n$.

Properties of $W(t)$ with the $\equiv$-sign are definitions. With respect to (2.4.37) the Langevin equation (2.4.35) can be written as

$$d\vec{x}(t) = \vec{A}(\vec{x},t)dt + \mathbf{B}(\vec{x},t)d\vec{W}(t), \tag{2.4.39}$$

where $\vec{W}(t)$ is a vector of independent Wiener processes. In a next step, Eq. (2.4.38) is used to replace $d\vec{W}(t)$ by a vector of random numbers from a standard normal distribution $\vec{Z} \in \mathcal{N}(0,1)$ multiplied by $\sqrt{dt}$

$$d\vec{x}(t) = \vec{A}(\vec{x},t)dt + \mathbf{B}(\vec{x},t)\vec{Z}\sqrt{dt}. \tag{2.4.40}$$

The stochastic calculus in this section is usually called Itô calculus, after the Japanese mathematician Kiyosi Itô. In the following section it is shown how to determine the still unknown parameters $\vec{A}$ and $\mathbf{B}$ by deriving the Fokker-Planck equation associated with (2.4.40).

2.4.2.2 The Fokker-Planck equation

An alternative to the SDE is to study stochastic processes by means of probability distribution functions $p(x,t)$. A stochastic process described by the Langevin equation (2.4.35) (i.e. Brownian motion) possesses the Markov property: given the one dimensional process $x(t)$, the values of x before a certain time t are irrelevant when predicting the future behaviour of x. This property is reflected by the probability distribution function for $x(t)$ written as $p(x,t|x_0,t_0)$ which gives the probability for the value x at t under the condition that it had the value x_0 at t_0. Stochastic processes which satisfy this property are called Markov processes. In general, the Fokker-Planck equation describes the evolution of the distribution function of a stochastic differential equation. Here it is shown how to obtain the Fokker-Planck equation for the Langevin equation (2.4.40) and its similarity to the advection-diffusion equation. The total derivative of an arbitrary function $f(x,t)$ is

$$\begin{aligned} df(x(t)) &= f(x(t)+dx(t)) - f(x((t)) \\ &= \frac{\partial f(x(t))}{\partial x}\, dx(t) + \frac{1}{2}\frac{\partial^2 f(x(t))}{\partial x^2}\, (dx(t))^2 + \cdots \end{aligned} \tag{2.4.41}$$

where $dx(t)$ is calculated by means of the Langevin equation (2.4.39)

$$dx(t) = A(x,t)dt + B(x,t)dW(t). \tag{2.4.42}$$

Substituting Eq. (2.4.42) into Eq. (2.4.41) and only taking into account the first two terms on the right-hand side yields

$$\begin{aligned} df(x(t)) &= (A(x,t)dt + B(x,t)dW(t))\ \frac{f(x(t))}{\partial x} \\ &+ \frac{1}{2}\underbrace{(A(x,t)dt + B(x,t)dW(t))^2}_{(dx(t))^2}\ \frac{\partial^2 f(x(t))}{\partial x^2}. \end{aligned} \tag{2.4.43}$$

Again, dt is an infinitesimal time step so that $(dt)^2 \approx 0$ and $dW\,dt \approx 0$. This allows us to write $(dx(t))^2$ as

$$\begin{aligned} (dx(t))^2 &= (A(x,t)\ dt + B(x,t)\ dW(t))^2 \\ &= A(x,t)^2\ (dt)^2 + 2\ A(x,t)\ B(x,t)\ dW(t)\ dt + B(x,t)^2\ (dW(t))^2 \\ &\approx B(x,t)^2\ (dW(t))^2 \end{aligned} \tag{2.4.44}$$

and Eq. (2.4.41) simplifies to

$$\begin{aligned} df(x(t)) &= (A(x,t)dt + B(x,t)dW(t))\ \frac{\partial f(x(t))}{\partial x} \\ &+ \frac{1}{2}B(x,t)^2\ (dW(t))^2\ \frac{\partial^2 f(x(t))}{\partial x^2}. \end{aligned} \tag{2.4.45}$$

In order to include a probability distribution function, the mean of Eq. (2.4.45) divided by dt is calculated

$$\begin{aligned} \left\langle \frac{df(x(t))}{dt} \right\rangle &= \left\langle \left(A(x,t) + B(x,t)\frac{dW(t)}{dt} \right)\ \frac{\partial f(x(t))}{\partial x} \right\rangle \\ &+ \left\langle \frac{1}{2}B(x,t)^2\ \frac{(dW(t))^2}{dt}\ \frac{\partial^2 f(x(t))}{\partial x^2} \right\rangle. \end{aligned} \tag{2.4.46}$$

From the properties of $W(t)$, it follows that $\left\langle \frac{dW(t)}{dt} = 0 \right\rangle$ and $\left\langle \frac{d^2W(t)}{dt} = 1 \right\rangle$ and Eq. (2.4.46) is reduced to

$$\left\langle \frac{df(x(t))}{dt} \right\rangle = \left\langle (A(x,t)\ \frac{\partial f(x(t))}{\partial x} \right\rangle + \left\langle \frac{1}{2}B(x,t)^2\ \frac{\partial^2 f(x(t))}{\partial x^2} \right\rangle. \tag{2.4.47}$$

The mean of $f(x(t))$ can as well be expressed in integral form

$$\langle f(x(t)) \rangle = \int f(x(t))\ p(x,t|x_0,t_0)dx \tag{2.4.48}$$

where $p(x,t|x_0,t_0)$ is the conditional probability distribution function. The total derivative of Eq. (2.4.48) is

$$\begin{aligned}\left\langle \frac{df(x(t))}{dt} \right\rangle &= \frac{d}{dt}\langle f(x(t))\rangle \\ &= \frac{d}{dt}\int f(x(t))\; p(x,t|x_0,t_0)dx \\ &= \int \frac{\partial}{\partial t}(f(x(t))\; p(x,t|x_0,t_0))\; dx \\ &= \int f(x(t))\; \frac{\partial}{\partial t}p(x,t|x_0,t_0)\; dx.\end{aligned} \tag{2.4.49}$$

Using Eq. (2.4.47), the integral can be written as (see *Gardiner* [1983])

$$\int f(x(t))\; \frac{\partial}{\partial t}p(x,t|x_0,t_0)\; dx$$

$$= \int \left((A(x,t)\; \frac{\partial f(x(t))}{\partial x} + \frac{1}{2}B(x,t)^2\; \frac{\partial f(x(t))}{\partial x}\; p(x,t|x_0,t_0) \right)\; dx. \tag{2.4.50}$$

Integration of the right-hand side by parts eliminates the derivations of $f(x)$ and yields

$$\int f(x(t))\; \frac{\partial}{\partial t}p(x,t|x_0,t_0)\; dx$$

$$\begin{aligned}&= \int \left(-\frac{\partial}{\partial x}\left(A(x,t)\; p(x,t|x_0,t_0)\right) \right. \\ &\left. + \frac{1}{2}\frac{\partial^2}{\partial x^2}\left(B(x,t)^2\; p(x,t|x_0,t_0)\right) \right) f(x)\; dx.\end{aligned} \tag{2.4.51}$$

However, $f(x)$ is an arbitrary function, so Eq. (2.4.50) is equal to

$$\begin{aligned}\frac{\partial}{\partial t}p(x,t|x_0,t_0) = &- \frac{\partial}{\partial x}\left(A(x,t)\; p(x,t|x_0,t_0)\right) \\ &+ \frac{1}{2}\frac{\partial^2}{\partial x^2}\left(\left(B(x,t)^2\; p(x,t|x_0,t_0)\right)\right.\end{aligned} \tag{2.4.52}$$

which is a Fokker-Planck equation for the conditional probability $p(x,t|x_0,t_0)$. The stochastic process $x(t)$ is determined equivalently by the Fokker-Planck equation (2.4.52) or the stochastic differential equation (2.4.39). For the n-dimensional case, the Fokker-Planck equation reads

$$\begin{aligned}\frac{\partial}{\partial t}p(\vec{x},t|\vec{x_0},t_0) = &- \sum_{i=1}^{n}\frac{\partial}{\partial x_i}\left(A_i(\vec{x},t)\; p(\vec{x},t|\vec{x_0},t_0)\right) \\ &+ \frac{1}{2}\sum_{i,j=1}^{n}\frac{\partial^2}{\partial x_i\, x_j}\left(\left(\mathbf{B}(\vec{x},t)\; \mathbf{B}^T(\vec{x},t)\right)_{ij}\; p(\vec{x},t|\vec{x_0},t_0)\right)\end{aligned} \tag{2.4.53}$$

where $\mathbf{B}^T$ is the transpose of matrix $\mathbf{B}$. Setting $n = 3$, $\vec{A} = (u, v, w)$, $\frac{1}{2}\mathbf{B}\mathbf{B}^T = \begin{bmatrix} A_x & 0 & 0 \\ 0 & A_y & 0 \\ 0 & 0 & \nu' \end{bmatrix}$ and $p(\vec{x}, t|\vec{x_0}, t_0) = C(\vec{x}, t)$ the Fokker-Planck equation becomes

$$\frac{\partial C}{\partial t} + \nabla \cdot (\vec{u}\, C) = \frac{\partial^2}{\partial x^2}(A_x\, C) + \frac{\partial^2}{\partial y^2}(A_y\, C) + \frac{\partial^2}{\partial z^2}(\nu'\, C) \tag{2.4.54}$$

which is similar to the three-dimensional advection-diffusion equation (2.2.37)

$$\frac{\partial C}{\partial t} + \nabla \cdot (\vec{u}\, C) = \frac{\partial}{\partial x}\left(A_x \frac{\partial C}{\partial x}\right) + \frac{\partial}{\partial y}\left(A_y \frac{\partial C}{\partial y}\right) + \frac{\partial}{\partial z}\left(\nu' \frac{\partial C}{\partial z}\right). \tag{2.4.55}$$

The apparent difference between both equations (at the right-hand side) and its meaning for modelling diffusion with the Fokker-Planck equation (2.4.54) will be discussed in the next section.

2.4.2.3 Modelling diffusion with random walk

A random walk model consisting of a large number of statistically independent steps is suitable to represent the chaotic nature of turbulent diffusion. The size of the diffusive step is determined by the stochastic differential equation (2.4.35) whose unknown quantities have been determined in the last section as

$$\vec{A}(\vec{x}, t) = (u(\vec{x}, t), v(\vec{x}, t), w(\vec{x}, t)) \tag{2.4.56}$$

$$\mathbf{B} = \begin{bmatrix} \sqrt{2\, A_x} & 0 & 0 \\ 0 & \sqrt{2\, A_y} & 0 \\ 0 & 0 & \sqrt{2\, \nu'} \end{bmatrix}. \tag{2.4.57}$$

Now, it is possible to write down Eq. (2.4.40) as follows

$$d\vec{x}(t) = \begin{pmatrix} u(\vec{x}, t) \\ v(\vec{x}, t) \\ w(\vec{x}, t) \end{pmatrix} dt + \begin{bmatrix} \sqrt{2\, A_x} & 0 & 0 \\ 0 & \sqrt{2\, A_y} & 0 \\ 0 & 0 & \sqrt{2\, \nu'} \end{bmatrix} \begin{pmatrix} Z_1 \\ Z_2 \\ Z_3 \end{pmatrix} \sqrt{dt}, \tag{2.4.58}$$

where Z_1, Z_2, Z_3 are independent random numbers from the standard normal distribution with zero mean and unit variance. Unfortunately, modelling turbulent diffusion with the Fokker-Planck equation is not realistic. *Visser*

[1997] showed that the random walk model based on Eq. (2.4.58) omitting the advective part, discretised as

$$x_{n+1} = x_n + Z_1\sqrt{2\ A_x(\vec{x}_n)\ \Delta t} \tag{2.4.59}$$

$$y_{n+1} = y_n + Z_2\sqrt{2\ A_y(\vec{x}_n)\ \Delta t} \tag{2.4.60}$$

$$z_{n+1} = z_n + Z_3\sqrt{2\ \nu'(\vec{x}_n)\ \Delta t} \tag{2.4.61}$$

tends to accumulate particles in regions of low diffusivity. Rewriting the Fokker-Planck equation (2.4.54) without the drift part gives

$$\begin{aligned}\frac{\partial C}{\partial t} &= \frac{\partial^2}{\partial x^2}(A_x\ C) + \frac{\partial^2}{\partial y^2}(A_y\ C) + \frac{\partial^2}{\partial z^2}(\nu'\ C)\\ \Leftrightarrow \frac{\partial C}{\partial t} &= \frac{\partial}{\partial x}\left(A_x\frac{\partial C}{\partial x}\right) + \frac{\partial}{\partial y}\left(A_y\frac{\partial C}{\partial y}\right) + \frac{\partial}{\partial z}\left(\nu'\frac{\partial C}{\partial z}\right)\\ &+ \frac{\partial}{\partial x}\left(\frac{\partial A_x}{\partial x}\ C\right) + \frac{\partial}{\partial y}\left(\frac{\partial A_y}{\partial y}\ C\right) + \frac{\partial}{\partial z}\left(\frac{\partial \nu'}{\partial z}\ C\right).\end{aligned} \tag{2.4.62}$$

The terms $\frac{\partial}{\partial x}\left(\frac{\partial A_x}{\partial x}\ C\right), \frac{\partial}{\partial y}\left(\frac{\partial A_y}{\partial y}\ C\right), \frac{\partial}{\partial z}\left(\frac{\partial \nu'}{\partial z}\ C\right)$ on the right-hand side which occur - in comparison to advection-diffusion Eq. (2.2.37) - additionally, represent an actual flux from areas of negative diffusivity curvature (i.e. a maximum in a diffusivity profile) to areas of positive diffusivity curvature (i.e. a minimum in a diffusivity profile) so that unrealistic un-mixing occurs. To remove this inconsistency, *Hunter et al.* [1993] added non-random advective components to the random walk scheme

$$x_{n+1} = x_n + \frac{\partial A_x(\vec{x}_n)}{\partial x}\Delta t + Z_1\sqrt{2\ A_x(\vec{x}_n)\ \Delta t} \tag{2.4.63}$$

$$y_{n+1} = y_n + \frac{\partial A_y(\vec{x}_n)}{\partial y}\Delta t + Z_2\sqrt{2\ A_y(\vec{x}_n)\ \Delta t} \tag{2.4.64}$$

$$z_{n+1} = z_n + \frac{\partial \nu'(\vec{x}_n)}{\partial z}\Delta t + Z_3\sqrt{2\ \nu'(\vec{x}_n\ \Delta t}. \tag{2.4.65}$$

The additional terms represent a flux from areas of negative diffusivity curvature to areas of positive diffusivity curvature (as it would be expected from a given diffusivity profile) and the numerical scheme (2.4.63)-(2.4.65) simulates turbulent diffusion corresponding to the situation described by the Fickian diffusion equation (2.2.37) without the physically unrealistic un-mixing tendency.

2.4.2.4 Implementation

The random walk model implemented into GETM and GOTM is based on the scheme proposed by *Hunter et al.* [1993]. A diffusive step is carried out each macro time step Δt for the internal mode of GETM and the particle position is updated according to (2.4.63)-(2.4.65) with a slight modification: the random numbers Z_1, Z_2, Z_3 are not taken from the standard normal distribution but from a uniform distribution with zero mean and a variance of $\frac{1}{3}$ (i.e. the uniform random numbers vary between $+1$ and -1). According to the Lindeberg-Feller central limit theorem (*Feller* [1935]) the distribution of a normal form variate

$$Z_{norm} = \frac{Z}{\sqrt{\langle (Z - \langle Z \rangle)^2 \rangle}}, \tag{2.4.66}$$

where Z is a random variable with zero mean and finite variance $\langle (Z - \langle Z \rangle)^2 \rangle$, tends to the normal distribution with zero mean and unit variance $\mathcal{N}(0, 1)$. In order to include $Z_{norm} = Z/\sqrt{1/3}$ the random walk model (2.4.63)-(2.4.65) becomes

$$x_{n+1} = x_n + \frac{\partial A_x(\vec{x}_n)}{\partial x}\Delta t + Z_1\sqrt{6\ A_x(\vec{x}_n)\ \Delta t} \tag{2.4.67}$$

$$y_{n+1} = y_n + \frac{\partial A_y(\vec{x}_n)}{\partial y}\Delta t + Z_2\sqrt{6\ A_y(\vec{x}_n)\ \Delta t} \tag{2.4.68}$$

$$z_{n+1} = z_n + \frac{\partial \nu'(\vec{x}_n)}{\partial z}\Delta t + Z_3\sqrt{6\ \nu'(\vec{x}_n)\ \Delta t}. \tag{2.4.69}$$

In the application of the random walk model to the Wadden Sea, horizontal diffusion is not included. The horizontal diffusivities A_x, A_y are set to zero since the shear dispersion (combination of vertical mixing and shear) is the major horizontal dispersion mechanism. The vertical diffusivity ν' is calculated by the turbulence model using the Kolmogorov-Prandtl relation (*Burchard and Bolding* [2002])

$$\nu' = c_\mu^{'}\frac{k^2}{\varepsilon}. \tag{2.4.70}$$

Here, k is the turbulent kinetic energy, ε is the dissipation rate, and $c_\mu^{'}$ is a so-called stability function depending on shear, stratification and turbulent time scale, $\tau = k/\varepsilon$. The vertical eddy diffusivity is located on the Eulerian grid at the position of the vertical velocity component w. Therefore it is easy to linearly interpolate ν' to the instantaneous vertical position z_n of a tracer in the grid box with index (i, j, k) and update the position according

to the discretised formulation of Eq. (2.4.69)

$$z_{n+1} = z_n + \frac{\nu'(i,j,k) - \nu'(i,j,k-1)}{h(i,j,k)}\Delta t + Z_3\sqrt{6\ \nu'(z_n)\ \Delta t} \tag{2.4.71}$$

where $h(i,j,k)$ is the depth of the k^{th} layer at the horizontal position denoted by (i,j) on the model grid.

Chapter 3

Idealised testcases

This chapter deals with the idealised computer simulations which have been conducted to understand the Lagrangian advection and diffusion algorithms and to guarantee the proper implementation into GOTM and GETM.

3.1 2D: Horizontal advection

As a first test of the advection algorithm, a simple two-dimensional test case has been developed. The advection algorithm has been implemented as a stand-alone model and simulations have been carried out with one particle being transported in a stationary velocity field. In addition, the Runge-Kutta method has been used to model advection.

3.1.1 Model setup

The model domain is a square of length $L = 100\,\mathrm{m}$ which ranges from $[-50\,\mathrm{m}, 50\,\mathrm{m}]$ in both directions. The grid spacing is $\Delta x = \Delta y = 1\,\mathrm{m}$ and the temporal resolutions for the advection model are chosen as $\Delta t = 0.001\,\mathrm{s}$ and $\Delta t = 0.01\,\mathrm{s}$, respectively. The stationary velocity field depends on x and y and the components of the velocity vector are calculated on an Arakawa C-grid according to

$$u(x,y) = \frac{1}{2}\omega \cdot x + \omega \cdot y \tag{3.1.1}$$

$$v(x,y) = -\omega \cdot x - \frac{1}{2}\omega \cdot y \tag{3.1.2}$$

where $\omega = \frac{2\pi}{\mathrm{s}}$ is the angular velocity. In this velocity field, a particle moves clockwise on a closed path which has the form of an ellipse (see Appendix

A). To exemplarily show the difference between the analytical advection scheme and a numerical discretisation method, the fourth order Runge-Kutta method is implemented additionally to model the advection equation. The fourth order Runge-Kutta method is often used to numerically solve ordinary differential equations and is considered to provide a good balance of power, precision and simplicity to program. It uses four evaluations of u, v during a time step Δt (*Press et al.* [1996])

$$u_1 = u(x_n, y_n) \qquad v_1 = v(x_n, y_n) \tag{3.1.3}$$

$$u_2 = u(x + \frac{1}{2}\Delta t\, u_1, y + \frac{1}{2}\Delta t\, v_1) \qquad v_2 = v(x + \frac{1}{2}\Delta t\, u_1, y + \frac{1}{2}\Delta t\, v_1) \tag{3.1.4}$$

$$u_3 = u(x + \frac{1}{2}\Delta t\, u_2, y + \frac{1}{2}\Delta t\, v_2) \qquad v_3 = v(x + \frac{1}{2}\Delta t\, u_2, y + \frac{1}{2}\Delta t\, v_2) \tag{3.1.5}$$

$$u_4 = u(x + \Delta t\, u_3, y + \Delta t\, v_3) \qquad v_4 = v(x + \Delta t\, u_3, y + \Delta t\, v_3) \tag{3.1.6}$$

and updates the particle position as follows

$$x_{n+1} = x_n + \frac{1}{6}\Delta t\ (u_1 + 2\,u_2 + 2\,u_3 + u_4) + \mathcal{O}(\Delta t)^5 \tag{3.1.7}$$

$$y_{n+1} = y_n + \frac{1}{6}\Delta t\ (v_1 + 2\,v_2 + 2\,v_3 + v_4) + \mathcal{O}(\Delta t)^5 \tag{3.1.8}$$

where $\mathcal{O}(\Delta t)^5$ is the order of the truncation error. The initial position of the particle is $x_0 = y_0 = 10\,\mathrm{m}$ and the simulations are carried out for a period of 1.15 s which is approximately the time a particle needs to perform one complete revolution.

3.1.2 Results

The computed trajectories for the analytical and the Runge-Kutta method are shown in Fig. (3.1.2) together with the exact orbit according to the analytical solution (A.0.15). It is apparent that the particle path, calculated by the analytical method with respect to crossing of cell boundaries during a time step Δt, is independent of the size of the time step. In contrast to that, the particle positions obtained from the Runge-Kutta method become more inaccurate as the time step is increased. Of course, the precision of the Runge-Kutta method can be improved by applying correction methods such as the adaptive step size algorithm, but this will not be discussed here any further.

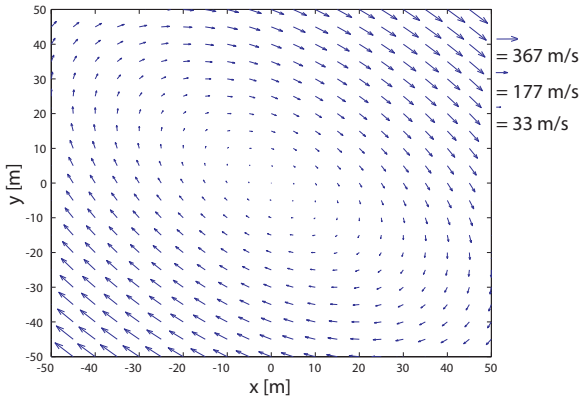

Fig. 3.1.1: Velocity field for the two-dimensional advection case.

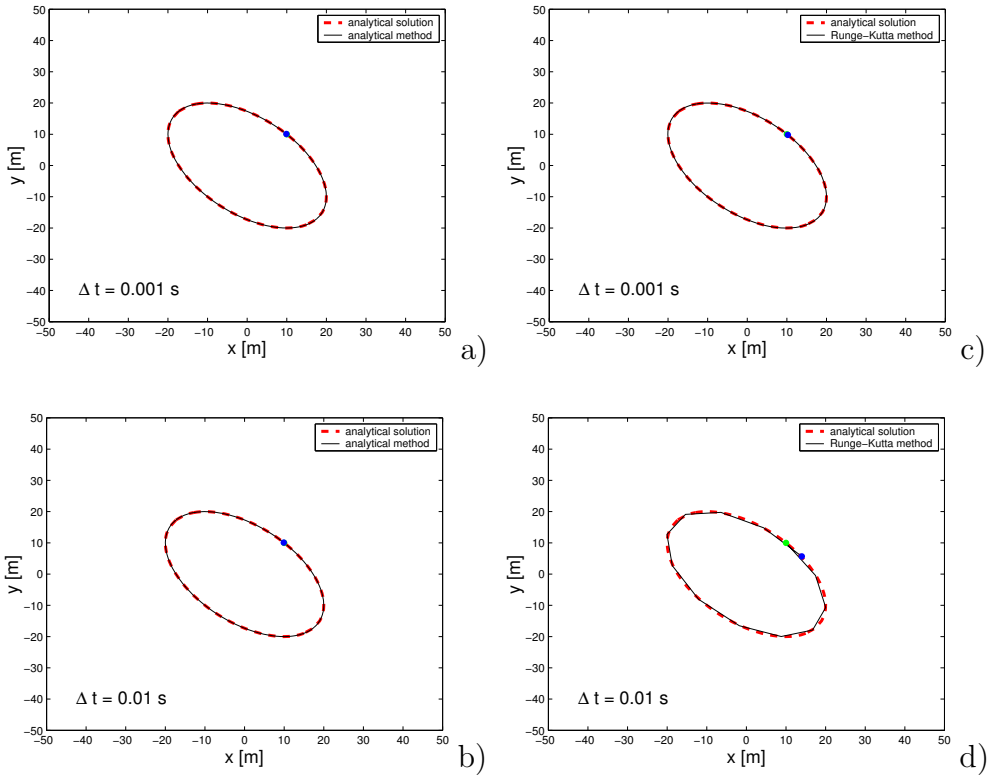

Fig. 3.1.2: Particle trajectories computed from the analytical and the Runge-Kutta algorithm for two different time steps $\Delta t = 0.001$ s and $\Delta t = 0.01$ s.

3.2 1D: Vertical sediment transport

In this section results are presented from modelling sediment suspension and transport with GOTM in a one-dimensional water column (z-direction). To compute the vertical sediment profile, a Eulerian scheme and the random walk model are used. The results are compared with the analytical solution

of the advection-diffusion equation for sediment. The simulations are carried out under idealised conditions. To simplify the momentum equation rotational and viscous effects are neglected. The pressure gradient is constant over the whole water column resulting in a shear stress decreasing linear towards the surface. Under these conditions, the momentum equation, the relation of Kolmogorov and Prandtl, the k-equation and the ε-equation form a closed system of equations (*Burchard et al.* [1999])

$$\nu_t \frac{\partial u}{\partial z} = (u_*^b)^2 \left(1 - \frac{z}{D}\right) \tag{3.2.1}$$

$$L(z) = \kappa(z + z_0) \left(1 - \frac{z}{D}\right)^{\frac{1}{2}} \tag{3.2.2}$$

$$P = \varepsilon \tag{3.2.3}$$

$$\nu_t = c_\mu^0 \sqrt{k} L \tag{3.2.4}$$

where z_0 is the roughness length, D is the water depth and u_*^b denotes the bottom friction velocity. With $u(z = 0) = 0$, the analytical solution of the system of equations (3.2.1) - (3.2.4) for momentum is the log-law

$$\frac{u(z)}{u_*} = \frac{1}{\kappa} \ln \left(\frac{z + z_0}{z_0}\right). \tag{3.2.5}$$

The solution for the turbulent kinetic energy k is a linearly decreasing profile towards the surface,

$$k(z) = \left(\frac{u_*^b}{c_\mu^0}\right)^2 \left(1 - \frac{z}{D}\right), \tag{3.2.6}$$

such that the result for the eddy viscosity is a parabolic profile

$$\nu_t(z) = \kappa u_*^b (z + z_0) \left(1 - \frac{z}{D}\right). \tag{3.2.7}$$

3.2.1 The Rouse profile

Transport of sediment grains in the vertical is described by the advection-diffusion equation

$$\frac{\partial C_{Sed}}{\partial t} + (w - w_{Sed}) \frac{\partial C_{Sed}}{\partial z} = \frac{\partial}{\partial z} \left((D_{Sed} + \nu_t') \frac{\partial C_{Sed}}{\partial z}\right) \tag{3.2.8}$$

where w_{Sed} is the fall velocity of sediment particles and D_{Sed}, ν_t' are the coefficients of molecular diffusion of sediment and eddy diffusivity, respectively. The solution of Eq. (3.2.8) can be obtained by neglecting molecular diffusion and taking into account that in a steady state $dC_{Sed}/dt =$

$\partial C_{Sed}/\partial t + w\ \partial C_{Sed}/\partial z = 0$ so that Eq. (3.2.8) reduces to

$$\frac{\partial}{\partial z}\left(\nu_t'\,\frac{\partial C_{Sed}}{\partial z} + w_{Sed}\,C_{Sed}\right) = 0$$

$$\Leftrightarrow \nu_t'\,\frac{\partial C_{Sed}}{\partial z} + w_{Sed}\,C_{Sed} = const. = 0. \tag{3.2.9}$$

Eq. (3.2.9) represents a balance between the rate of settling $w_{Sed}\ C_{Sed}$ and the rate of turbulent diffusion $\nu_t'\ \partial C_{Sed}/\partial z$. Integration of the balance equation results in the expression for the concentration profile $C(z)$, first derived by Hunter Rouse (*Rouse* [1937])

$$C(z) = C_a \exp\left(-w_{Sed}\int_a^z \frac{1}{\nu_t'}\,dz\right) \tag{3.2.10}$$

where C_a is the reference concentration at the arbitrary level z_a which is usually chosen to be close to the sediment bed. The reference concentration C_a has to be known for the calculation of the concentration profile. It is assumed that the eddy diffusivity ν_t' is proportional to the eddy viscosity ν_t and can be calculated from

$$\nu_t' = \frac{\nu_t}{\sigma_t} \tag{3.2.11}$$

where $\sigma_t \approx 0.7$ is the constant Prandtl number. The sediment profile (3.2.10) with respect to (3.2.7) and (3.2.11) is

$$\begin{aligned} C(z) &= C_0 \exp\left(-\sigma_t \frac{w_{Sed}}{\kappa u_b^*}\int_{z_0}^z \frac{1}{(z+z_0)\left(1-\frac{z}{D}\right)}\,dz\right) \\ &= C_0 \exp\left(-\sigma_t \frac{w_{Sed}}{\kappa u_b^*}\ln\left(\frac{z+z_0}{z_0}\frac{D-z_0}{D-(z+z_c)}\right)\right). \end{aligned} \tag{3.2.12}$$

The reference concentration C_0 is computed at the roughness length at the bottom z_0

$$z_0 = 0.1\frac{\nu}{u_*^b} + 0.03 h_0^b \tag{3.2.13}$$

where ν is the eddy viscosity and h_0^b represents the height of the bottom roughness elements. Following *Smith and McLean* [1977], the bottom sediment concentration C_0 is a function of the bottom friction velocity and the critical friction velocity u_*^c (at which sediment particles begin to go into suspension)

$$C_0 = \gamma_1 \left(\frac{u_*^b}{u_*^c}\right)^2 \left[1 - \left(\frac{u_*^c}{u_*^b}\right)^2\right] \tag{3.2.14}$$

where $\gamma_1 = 1.56 \cdot 10^{-3}$ is a constant. The steady state solution (3.2.12) is the so-called Rouse profile and $w_{Sed}/(\kappa u_b^*)$ is the Rouse number.

3.2.2 Model setup

The water column has a depth of $D = 10\,\mathrm{m}$ and is divided into 100 equidistant intervals h_k. The indexing is upwards with $k = 1$ for the bottom layer and $k = N = 100$ for the surface layer. The time step is chosen to be $dt = 10\,\mathrm{s}$ and the simulation time is 12 hours in order to obtain quasi stationary profiles. The vertical transport of sediment is only due to settling of sediment particles and the turbulent diffusion

$$\frac{\partial C}{\partial t} - \frac{\partial}{\partial z}(w_s\, C + \nu_t' \frac{\partial}{\partial z} C) = 0. \tag{3.2.15}$$

In GOTM, the diffusive transport and the fall of sediment grains are treated separately from each other. For the diffusive transport, the layer integrated diffusion equation (3.2.15) is used (*Burchard and Bolding* [2002])

$$\int_{k-1}^{k} \frac{\partial C}{\partial t} - \frac{\partial}{\partial z}(\nu_t' \frac{\partial C}{\partial z}) dz = 0$$

$$\Leftrightarrow \frac{\partial h_k C}{\partial t} - \left(\nu_t' \frac{\partial C}{\partial z}\right)\Big|_k + \left(\nu_t' \frac{\partial C}{\partial z}\right)\Big|_{k-1} = 0. \tag{3.2.16}$$

At the surface and at the bottom, the Neumann-type boundary conditions are

$$\left(\nu_t' \frac{\partial C}{\partial z}\right)\Big|_{k=N} = F_s = 0 \tag{3.2.17}$$

and

$$\left(\nu_t' \frac{\partial C}{\partial z}\right)\Big|_{k=0} = -F_b \tag{3.2.18}$$

where F_b and F_s are the turbulent boundary fluxes. The semi-implicit discretisation of (3.2.16) is written as follows:

$$\frac{h_N^{n+1} C_N^{n+1} - h_N^n C_N^n}{\Delta t} + \nu_{N-1}^n \frac{C_N^{n+\lambda} - C_{N-1}^{n+\lambda}}{\frac{1}{2}(h_N^{n+\lambda} - h_{N-1}^{n+\lambda})} = 0; \qquad k = N \tag{3.2.19}$$

$$\begin{aligned} \frac{h_k^{n+1} C_k^{n+1} - h_k^n C_k^n}{\Delta t} &- \nu_k^n \frac{C_{k+1}^{n+\lambda} - C_k^{n+\lambda}}{\frac{1}{2}(h_{k+1}^{n+\lambda} - h_k^{n+\lambda})} \\ &+ \nu_{k-1}^n \frac{C_k^{n+\lambda} - C_{k-1}^{n+\lambda}}{\frac{1}{2}(h_k^{n+\lambda} - h_{k-1}^{n+\lambda})} = 0; \qquad 1 < k < N \end{aligned} \tag{3.2.20}$$

$$\frac{h_1^{n+1}C_1^{n+1} - h_1^n C_1^n}{\Delta t} - \nu_1^n \frac{C_2^{n+\lambda} - C_1^{n+\lambda}}{\frac{1}{2}(h_2^{n+\lambda} - h_1^{n+\lambda})} - F_b = 0; \qquad k = 1 \tag{3.2.21}$$

with

$$C_k^{n+\lambda} = \lambda C_k^{n+1} + (1-\lambda) C_k^n \tag{3.2.22}$$

and

$$h_k^{n+\lambda} = \lambda h_k^{n+1} + (1-\lambda) h_k^n. \tag{3.2.23}$$

Here, upper indices denote time levels and lower indices stand for the vertical discrete location. The Crank-Nicholson parameter is λ, such that for $\lambda = 0$ a fully explicit, for $\lambda = 1$ a fully implicit scheme and for $\lambda = 0.5$ the Crank-Nicholson second-order in time scheme is obtained. This numerical scheme leads to a system of linear equations in the form of a matrix equation. The tridiagonal matrix of this equation is solved by means of the simplified Gaussian elimination. The constant fall of sediment is modelled by using a directional splitting method (i.e. applying a 1-D scheme in one direction at a time) and a Total Variation Diminishing (TVD) advection scheme (*Pietrzak* [1998], see *Burchard and Bolding* [2002] for details).

3.2.2.1 Modelling sediment suspension

For parameterisation, the sediment has a density of $\rho_{Sed} = 2650\,\mathrm{kg/m^3}$ and the sediment particles are assumed to be sphere-like with a diameter of $d = 62.5 \cdot 10^{-6}\,\mathrm{m}$, a volume of $V = 4/3\pi(d/2)^3 = 1.28 \cdot 10^{-13}\,\mathrm{m^3}$ and a mass of $m = 3.3875 \cdot 10^{-10}\,\mathrm{kg}$. The fall velocity w_s for sphere-shaped particles is calculated using the equation proposed by Zanke (*Zanke* [1977])

$$w_s = 10\frac{\nu}{d}\left(\sqrt{1 + \frac{0.01\,g'\,d^3}{\nu^2}} - 1\right) \tag{3.2.24}$$

where ν is the molecular viscosity of water and g' is the reduced gravity

$$g' = g\frac{\rho_{Sed} - \rho_0}{\rho_0} \tag{3.2.25}$$

with ρ_0 being the standard reference density. First, the Rouse profile is computed with the semi-implicit Eulerian scheme for diffusion and the TVD scheme for advection in order to obtain the steady-state concentration of suspended sediment. After a simulation time of 12 hours, the total sediment concentration is $C_{total} = 1.87 \cdot 10^{-2}\,kg/m^3$. This equals a number of

$55,472,000$ sediment particles suspended in the water column. The random walk model uses a number of $554,720$ tracers, each of them representing a load of sediment (not a sediment particle!) $l_{Sed} = 3.3875 \cdot 10^{-8}$ kg to compute the Rouse profile. Initially, all tracer particles are located at the sediment bed and their vertical position is updated with respect to turbulent diffusion and settling as

$$z^{n+1} = z^n + \frac{\nu_k^n - \nu_{k-1}^n}{h_k)}\Delta t + Z\sqrt{6\ \nu^n(z^n)\ \Delta t} - w_s\ \Delta t \tag{3.2.26}$$

where Z is a uniform random number with zero mean and a variance of $1/3$. To show the difference between the correct random walk model (3.2.26) and the physically wrong approach (2.4.61), another simulation is carried out where the tracer positions are updated according to

$$z^{n+1} = z^n + Z\sqrt{6\ \nu^n(z^n)\ \Delta t} - w_s\ \Delta t. \tag{3.2.27}$$

At the end of a simulation with one of the random walk models, the number of tracers in each layer is computed and multiplied by the load of sediment l_{Sed} to obtain the stationary sediment profiles.

3.2.3 Results

The simulations are carried out for a period of 12 hours and the vertical profiles of u, k, ε, ν_t', ν_t shown in Fig. 3.2.1a - 3.2.1d are in conformance with the analytical solutions mentioned earlier. The turbulent kinetic energy k decreases linearly towards the surface as the influence of the bottom friction and the roughness of the sediment bed on the flow diminishes. The energy dissipation rate increases towards the bed where the dissipation has its maximum in the bottom boundary layer. The vertical profiles of the viscosity and the diffusivity are both parabolic and differ only by the constant factor σ_t. The sediment profile calculated by the Eulerian scheme is in good agreement with the analytical solution and shows a smooth exponential decrease with depth (Fig. 3.2.2a). The vertical profile obtained with the correct random walk model also reproduces the analytical solution, but shows small random errors (Fig. 3.2.2b). In contrast to that, the physically unrealistic random walk model tends to accumulate particles in areas of low diffusivity and leads to an overestimation of the sediment concentration close to the bottom and the surface as shown in Fig. (3.2.2c). The good agreement between the Eulerian scheme, the correct random walk model and the analytical solution is shown for ten different depths in Tab. 3.2.1.

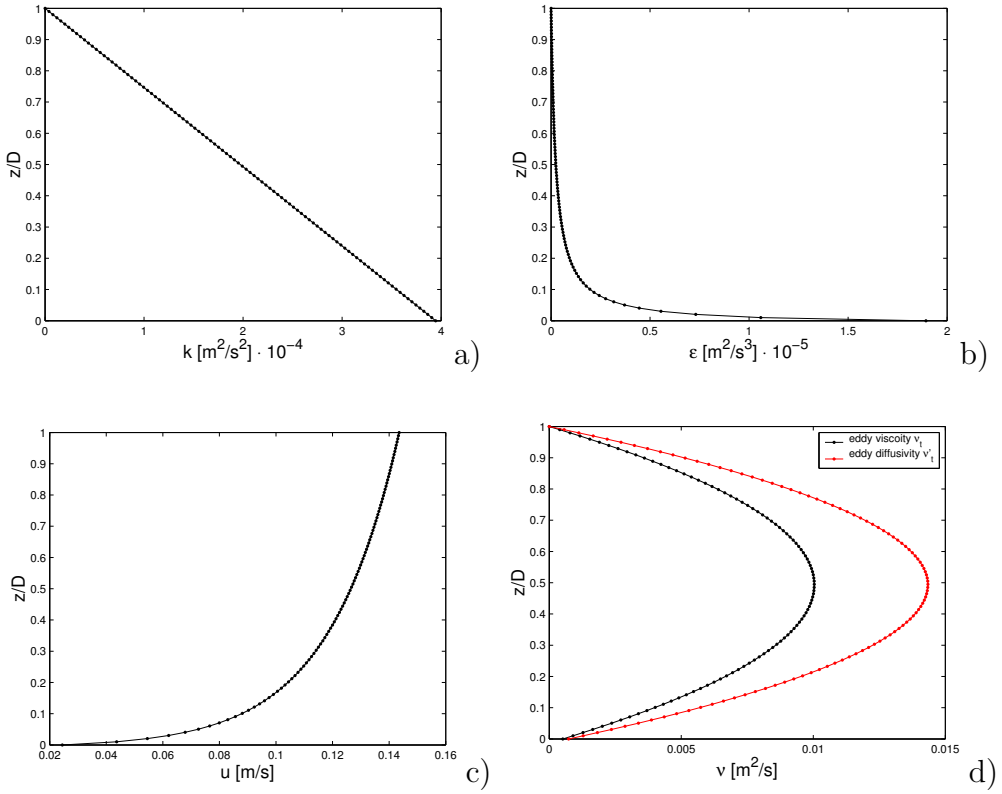

Fig. 3.2.1: Vertical profiles of a) the turbulent kinetic energy k, b) the energy dissipation rate ε, c) the zonal velocity component u and d) the eddy diffusivity ν_t' and viscosity ν_t.

Depth z [m]	$C_{Sed,Euler}$[kg/m^3]	$C_{Sed,Lagrange}$[kg/m^3]	$C_{Sed,analytical}$[kg/m^3]
-0.5	$1.03 \cdot 10^{-3}$	$1.07 \cdot 10^{-3}$	$1.04 \cdot 10^{-3}$
-1.5	$3.69 \cdot 10^{-4}$	$3.59 \cdot 10^{-4}$	$3.62 \cdot 10^{-4}$
-2.5	$2.65 \cdot 10^{-4}$	$2.63 \cdot 10^{-4}$	$2.59 \cdot 10^{-4}$
-3.5	$2.13 \cdot 10^{-4}$	$2.14 \cdot 10^{-4}$	$2.09 \cdot 10^{-4}$
-4.5	$1.78 \cdot 10^{-4}$	$1.72 \cdot 10^{-4}$	$1.70 \cdot 10^{-4}$
-5.5	$1.51 \cdot 10^{-4}$	$1.49 \cdot 10^{-4}$	$1.47 \cdot 10^{-4}$
-6.5	$1.28 \cdot 10^{-4}$	$1.23 \cdot 10^{-4}$	$1.25 \cdot 10^{-4}$
-7.5	$1.07 \cdot 10^{-4}$	$1.05 \cdot 10^{-4}$	$1.05 \cdot 10^{-4}$
-8.5	$8.64 \cdot 10^{-5}$	$8.74 \cdot 10^{-5}$	$8.40 \cdot 10^{-5}$
-9.5	$6.28 \cdot 10^{-5}$	$6.41 \cdot 10^{-5}$	$6.10 \cdot 10^{-5}$

Table 3.2.1: Sediment concentrations at ten different depths calculated by the Eulerian scheme, the correct random walk model and the analytical solution.

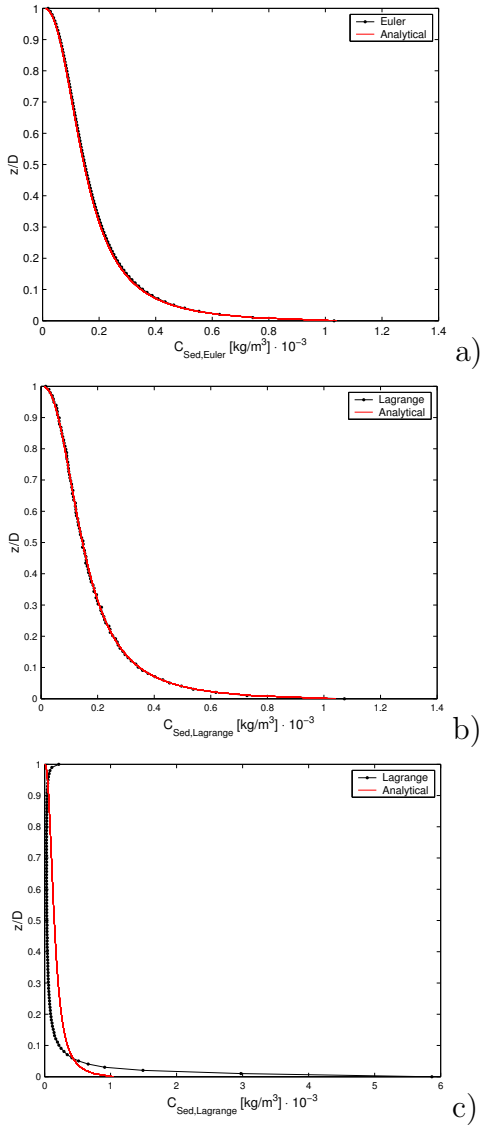

Fig. 3.2.2: Sediment profiles computed by three different models: a) semi-implicit Eulerian scheme for diffusion and a TVD-scheme for advection, b) correct random walk scheme according to *Hunter et al.* [1993], c) physically unrealistic random walk mentioned by *Visser* [1997]

3.3 2D: Advection and diffusion - wind-driven circulation

A test case has been conducted to simulate wind-driven circulation in a two-dimensional, continuously stratified lake using GETM. First, the model is run without the random walk algorithm in order to check the consistency of the advection scheme implemented into GETM. In a second run, the influence of turbulent diffusion on the particle path is included.

3.3.1 Model setup

The lake covers a length of $L_x = 2000\,\mathrm{m}$ and has a parabolic depth profile with a maximum depth of $D = 10\,\mathrm{m}$ at $x = 1000$ m. The domain has been discretised using 101 grid points in x-direction with a grid spacing $\Delta x = 20\,\mathrm{m}$ and 100 interface layers in the vertical using general vertical coordinates. The simulations are carried out with a micro time step $\Delta t_m = 1\,\mathrm{s}$ and a macro time step $\Delta t = 10\,\mathrm{s}$. As a forcing for the model, a constant wind stress $\tau_x = 0.375\,\mathrm{N/m^2}$ is applied. After a simulation time of one hour, the lake is in steady state equilibrium and a number of ten tracer particles is distributed equidistantly over depth in the middle of the lake. The simulations are carried out for another 23 hours and the particle paths are computed. For the advection and the advection-diffusion simulations, the same starting positions are used.

3.3.2 Results

In steady state equilibrium, the surface of the lake is slightly inclined to the west due to wind forcing, and the surface elevation ζ is higher at the east end of the lake where down-welling occurs (see Fig. 3.3.1a). The wind-induced circulation pattern in the lake consists of a large gyre which causes particles to move clockwise (see Fig. 3.3.1b). The vertical profiles for the eddy diffusivity and viscosity are depicted in Fig. 3.3.1c and 3.3.1d for three different positions along the length of the lake. All profiles have a parabolic shape and their maximum value increases from both ends towards the middle of the lake where diffusivity and viscosity have the most distinct profile. The trajectories of all particles are closed for the pure advection case as shown in Fig. 3.3.2a - 3.3.2c for three different starting positions. This leads to the conclusion that the advection algorithm is implemented properly. For the advection-diffusion case, the particle motions show a strong influence of turbulence. The drift patterns calculated for the same starting positions used for the advection case are depicted in Fig. 3.3.2d - 3.3.2f.

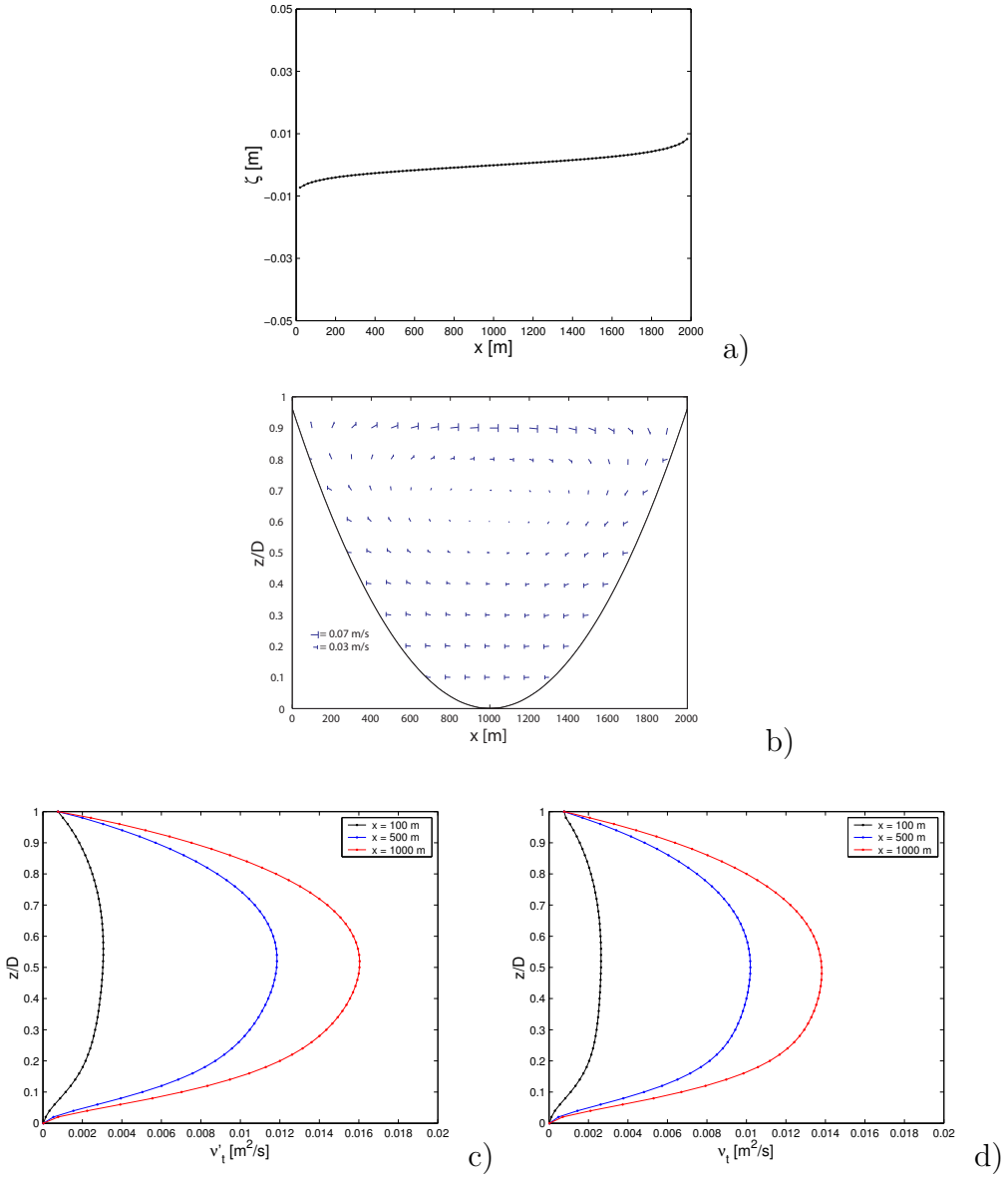

Fig. 3.3.1: Shown here is a) the sea surface elevation ζ along the length of the lake, b) the circulation pattern in the lake described by the velocity field, the vertical profiles of c) the eddy diffusivity ν_t' and d) the eddy viscosity ν_t at three different positions along the length of the lake.

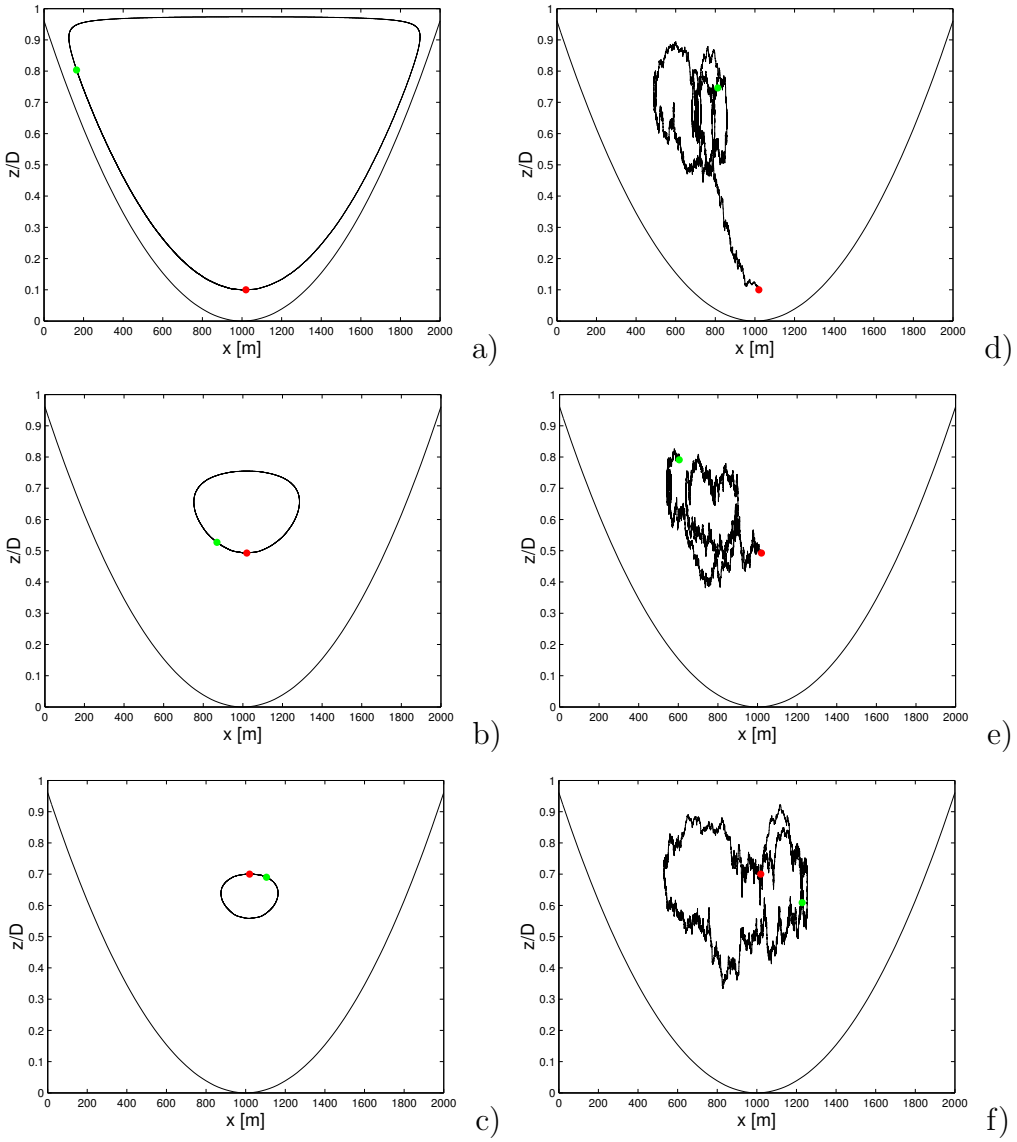

Fig. 3.3.2: Particle paths in a lake for three different vertical starting positions. The figures on the left side show the computed trajectories for the advection case and the figures on the right show the influence of turbulent diffusion on particle motions. The red dot marks the starting position of the particles and the green dot marks the position at the end of a model run. The particles in a) and d), b) and e), c) and f) have the same starting position.

Chapter 4

Realistic application

4.1 The model setup

4.1.1 The model domain

The Wadden Sea of the North Sea extends along a 500 km stretch between the Dutch Den Helder and the Danish Esbjerg with usually more than 10 km of width and a total area of about 9,300 km^2 (including islands). It is the largest coastal wetland in Europe consisting of mudflats, sandflats, saltmarshes and 23 barrier islands with sand dunes. The topography of the Wadden Sea is highly dynamic and geomorphologic processes working at all conceivable time and space scales result in a constantly changing landscape. About 4,500 km^2 of this area falls dry and gets flooded again twice a day by the tide through a system of tideways, channels and shipping channels between the islands. The major part of the Wadden Sea can be described as a mesotidal area with a tidal range between 1.4 m (Den Helder) and 3.5 m (Wilhelmshaven). The size of the barrier islands decreases towards areas with a tidal range greater than 2.9 m (inner German Bight) (QSR 1993). Approximately 56 % of the Wadden Sea stretches along the German Bight ranging from the island Borkum in front of the East Frisian coast to the island Sylt in front of the North Frisian coast as depicted in Fig. 4.1.1.
The area under investigation is located in the German part of the Wadden Sea region indicated by the square frame in Fig. 4.1.1. The model domain consists of the two islands Baltrum and Langeoog, the backbarrier basin between these islands and the East Frisian coast and a part of the open sea to the north of the islands (see Fig. 4.1.2). During the flooding phase North Sea water enters the model domain from the west and is transported into the basins through the narrow inlet Accumer Ee with speeds exceeding 1 m/s.

A_{total} [m^2] $\cdot 10^6$	88.56
A_h [m^2] $\cdot 10^6$	88.56
A_l [m^2] $\cdot 10^6$	41.38
D_h [m]	2.91
D_l [m]	1.89
V_h [m^3] $\cdot 10^6$	257.29
V_l [m^3] $\cdot 10^6$	82.60
ΔV [m^3] $\cdot 10^6$	174.69

Table 4.1.1: Volumes, areas, mean depths and tidal prism under spring tide conditions for the Langeoog basin. All values were calculated for the first day of the tidal forcing (19^{th} May 2000). A_{total} is the area of the basin without islands and coast, A_h and A_l are the areas covered with water at maximum flood and maximum ebb, respectively. V_h and V_l are the volumes corresponding to A_h and A_l. The tidal prism is denoted by ΔV.

The open ocean water fills the basin through the tidal channel and thereby gets mixed with coastal water masses from the last ebb phase and fresh water from Dornumer- and Bensersiel. During the ebb phase the mixed water masses leave the basin again through the inlet and most of the basin falls dry. With a horizontal resolution of 200 m, the topography of the model domain is more clearly identified in Fig. (4.1.3). The topographic map was created by Gerhard Geyer from the Institute for Coastal Research at the GKSS research centre using data from the Federal Waterways Engineering and Research Institute (BAW). The measuring points were separated by distances between 250 m at seaward locations and 20 m inside the channel between the two islands. In order to produce a map with a horizontal resolution of 200 m$\times$200 m all gaps in the values were filled without additional map material. The total area covers $237.12 \cdot 10^6$ m^2 with a number of 76 grid points in x-direction and 78 grid points in y-direction. The inter-tidal basin has a total area of $88.56 \cdot 10^6$ m^2 (without islands and coast). Inside the basin, the topographic height H ranges from 0.94 m above to -19.18 m below mean sea level with a mean of -1.51 m (indicated by the dotted line in Fig. 4.1.3). During maximum flood under spring tide conditions, the water covered area A_h in the basin is equal to the total area with a mean depth $D_h = 2.91$ m. The water volume is calculated as $V_h = 257.29 \cdot 10^6$ m^3. During low tide, the water mass of the inner basin has a volume of $V_l = 82.60 \cdot 10^6$ m^3 covering approximately half of the basin area with a mean water depth of $D_l = 1.89$ m (see Tab. 4.1.1).

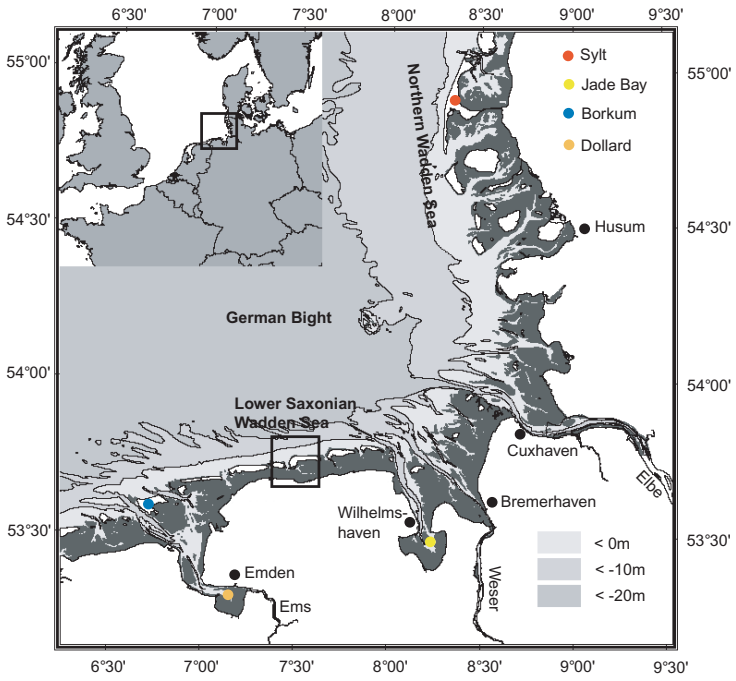

Fig. 4.1.1: The top left corner shows the North Sea, the location of the German Bight is indicated by the square frame. The other part of the figure depicts the German Bight in more detail. The model domain in the East Frisian Wadden Sea is marked by the frame between the islands Baltrum and Langeoog. The topographic map shows the area which becomes dry during ebb (darkest shading) and the area which is always covered with water (lightest shading). (modified after *Stanev et al.* [2003a])

4.1.2 The model forcing

The dominant physical driving forces in the Wadden Sea area are the tides, wind and wind waves. In this study, the forcing of the model is only due to the tides. Any effect of wind and wind waves is neglected.

The tide in the Wadden Sea area is dominated by the semi-diurnal lunar tide (M_2) with the well known period of 12.42 h (the latter often serves as a unit of time, denoted by T). The semi-diurnal solar tide (S_2) gives rise to the spring to neap tidal cycle. Spring tides are especially strong tides. They occur when the earth, the sun, and the moon are in a line. The gravitational forces of the moon and the sun both contribute to the tides. Spring tides occur during the full moon and the new moon. Neap tides are especially weak tides. They occur when the gravitational forces of the moon and the sun are perpendicular to one another (with respect to the earth). Neap tides occur during quarter moons.

For the model simulations, sea-level data from the operational model of

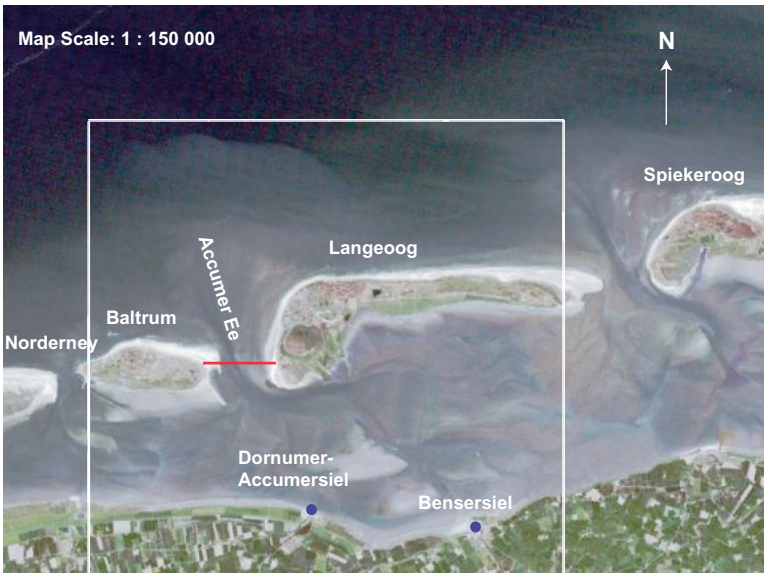

Fig. 4.1.2: Satellite image of the East Frisian Wadden Sea between Norderney and Spiekeroog. The model domain is indicated by the white frame. The intertidal basin between Baltrum and Langeoog is connected to the adjacent North Sea through the inlet Accumer Ee. The blue dots mark the areas of freshwater inflow through Dornumer- and Bensersiel. The red line approximately marks the transition from the shallow basin to the open Wadden Sea area. During the model runs, this line is used to determine the time when a Lagrangian tracer particle leaves the basin. The satellite image was taken from the web site of the GKSS (`http://w3k.gkss.de/data/dornum.html`) and was modified to include the labels of the islands, the inlet and the fresh water inflow.

the German Federal Maritime and Hydrographic Agency (Bundesamt für Seeschiffahrt und Hydrogaphie, BSH) are chosen (*Dick and Soetje* [1990]). The BSH-model is a three-dimensional prognostic model which simulates the North Sea and Baltic Sea with a horizontal resolution of 10 km, and the German Bight with a higher resolution of 1.8 km. The sea level data are calculated from the tidal constituents of 14 partial tides. When prescribing the boundary values for the sea surface elevation, the phase shift in the tidal rise and fall due to the amphidromy in the southern North Sea has to be taken into consideration. The tidal wave propagates through the North Sea as a Kelvin wave, in this case in a counter-clockwise circular motion. This leads to patterns of high and low tides rotating around amphidromic points at which the tidal rise and fall is zero. *Stanev et al.* [2003a] performed simulations for the whole East Frisian Wadden Sea with a model domain of 65 km length resulting in a phase shift of the tidal wave between the east and west boundaries of approximately 50 min. The length of the model area

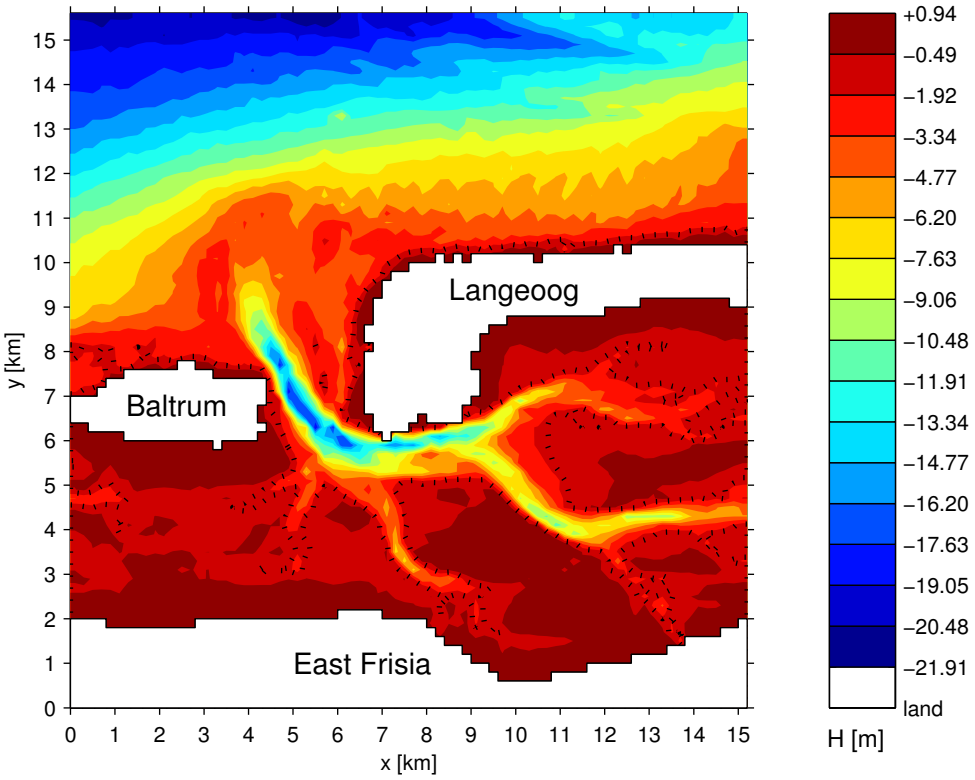

Fig. 4.1.3: Shown is the topography of the model domain. Most parts of the inter-tidal basin are shallower than −4 m. The mean topographic height inside the basin (−1.51 m) is indicated through the dotted line.

under investigation in this study is 15.2 km. For simplicity's sake, a linear relationship is assumed between the phase shift *Stanev et al.* [2003a] has applied and the phase shift for the length of the model area used in this study. Subsequently, the phase shift for the Baltrum-Langeoog area is taken to be 11.69 min.

In order to resolve this phase shift in the boundary values, two successive sea-level values in the data set have been interpolated linearly in time to yield a value with a lag of 11.69 min to the first value. These two values were allocated to the two northern corner points of the model area. Between these two values, a linear interpolation in space is carried out to obtain the boundary values along the northern boundary. The surface elevation along the western and eastern boundary is chosen to be the same as the first and last boundary value of the northern boundary, respectively.

The tidal forcing consists of the sea surface data from 19^{th} - 28^{th} May 2000 (see Fig. 4.1.4).

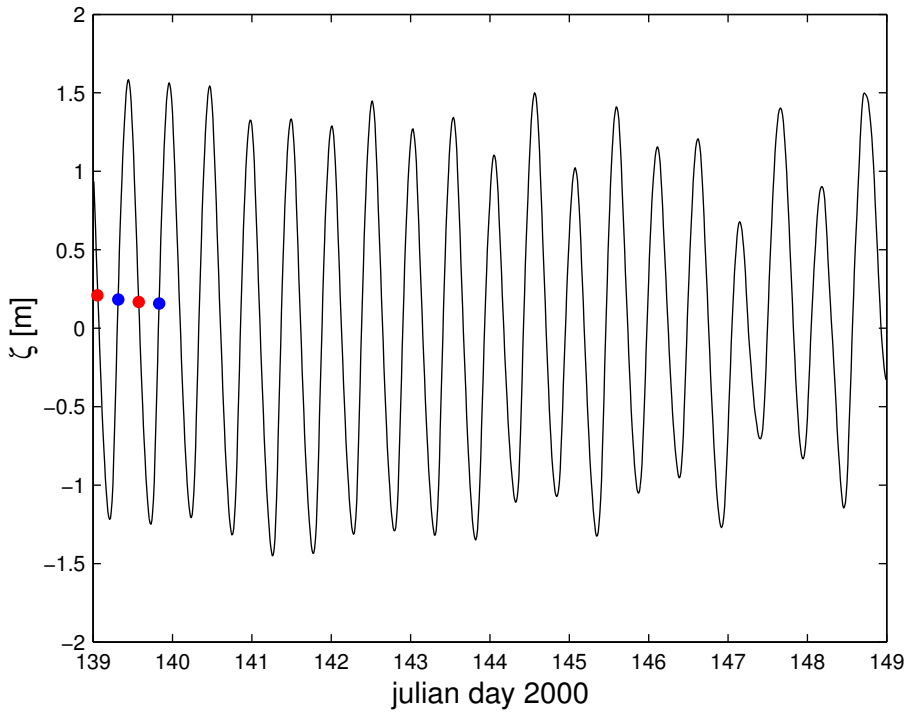

Fig. 4.1.4: Shown is the time series of the sea surface data used to force the model on the open boundaries. The red and blue dots mark the time of maximum ebb and flood current, respectively, on 19^{th} May 2000.

4.2 Modelling the residence time of the Langeoog basin

According to *Zimmerman* [1976] water residence times in estuaries and tidal basins are influenced by any factor that affects water movement, including freshwater inflow rates, tides, wind, mixing, stratification, and system topography. Since many of these factors are variable, residence times are also not static. This variability requires attention to the appropriate time interval over which the residence time should be expressed, and the representativeness of the conditions under which a given measurement is made. A long-term (seasonal or annual) average residence time is often most appropriate for the analysis of the effects of nutrients. Tides can be a major factor controlling estuary-ocean exchange of water and therefore water residence time. Important factors are the tidal range, tidal frequency (diurnal vs. semidiurnal) and basin depth. For a given area, residence times may vary over the spring-neap tide cycle.
As a final application of the Lagrangian tracer model, the residence time of the Langeoog basin is determined under realistic conditions taking into

account the tidal forcing of the Wadden Sea.

4.2.1 Transport time scales in natural basins

In the following, a brief description of the transport time scales in natural basins is given. In general, one has to distinguish between local and integral time scales. Local time scales depend on the initial position of a water parcel while integral time scales are obtained by averaging over the total number of water parcels inside the basin at a certain moment. The latter one can be derived from the first one but not vice versa.
The important time scales are
Age: Age is unique to each water parcel that enters a basin. It is defined as the time a parcel has spent inside the basin since entering it through one of the open boundaries (*Zimmerman* [1976]). Averaging over the ensemble of parcels leads to the age of the water mass of the basin.
Residence time: The time a water parcel needs from an arbitrary start location inside a basin to the outlet to the sea is called the residence time (*Zimmerman* [1976]).
Transit time: The transit time is the time a water parcel needs from the inlet to the outlet of a basin, thus it is the sum of age and residence time (*Zimmerman* [1976]). The transit time is often used as an integral time scale and compared with the mean age of the water parcels.
Flushing time: The flushing time is an integrative parameter. It characterises the water exchange of a basin and is defined as the ratio of the water volume of the basin to the flux through its boundaries. The mean flushing time is often calculated as the time necessary to reduce the initial mass of labelled water parcels to a fraction $1/e$ (e being the Eulerian number ≈ 2.718) (*Monsen et al.* [2002]). It can also be obtained from the tidal prism ΔV when only basin geometry and tidal range information are available. The approach assumes that tides exclusively flush the system. Flushing time using this approach is (*Dick and Schönfeld* [1996])

$$\tau_f = \frac{V_0}{\beta \, \Delta V} \tag{4.2.1}$$

where V_0 is the volume of the basin and β is a constant determined at 0.12 (*Ridderinkhof et al.* [1990]).
Turnover time: The turnover time is the spatial average of the residence time over the basin (*Deleersnijder and Tartinville* [1998]).

4.2.2 Numerical simulations

The residence time of the Langeoog basin is simulated by using GETM and the implemented particle tracking model. A total number of four simulations have been carried out, each of them starting either at maximum flood or maximum ebb current. According to *Ridderinkhof et al.* [1990] the residence time depends largely on the tidal phase at which the simulation is started and on the initial volume at starting time. When examining transport time scales, *Ridderinkhof et al.* [1990] proposes to start at mid-tide position which corresponds to about the time of maximum ebb or flood current. All four simulations start on 19^{th} May, 2000 and the exact starting times are shown in Fig. 4.1.4 and in Tab. 4.2.1. Each simulation is carried out over the full period of the tidal forcing data and the residence time is calculated on the last day of the tidal forcing (28^{th} May, 2000). The tidal forcing is mainly dominated by spring tide conditions, so that the results of the simulations are only representative for this type of tidal forcing. The model domain is initialised with a number of particles which represent the water volume in the basin at starting time V_0. The number of particles per grid box $n(i,j,k)$ is determined by its volume $V(i,j,k) = \Delta x\, \Delta y\, h(i,j,k)$ in the following way

$$n(i,j,k) = \text{int}\left(\frac{V(i,j,k)}{V_t}\right) \tag{4.2.2}$$

where $V_t = 1000\ \text{m}^3$ is the volume represented by one tracer particle in the above equation. In order to even cover the basin areas with a volume smaller than V_t a minimum value of $n(i,j,k) = 2$ is introduced. This means that one particle is likely to account for a volume smaller than V_t. It should be noted that even dry areas are initialised with particles and the residence time is determined from the point on when these grid boxes are flooded again. Throughout all simulations a macro time step $\Delta t = 40\,\text{s}$ and a micro time step $\Delta t = 8\,\text{s}$ is used. The vertical domain is discretised using a number of ten vertical layers. The drying and flooding parameter is chosen in accordance with the Sylt-Rømø Bight test case developed by *Burchard and Bolding* [2002], $D_{crit} = 0.2\,\text{m}$ and $D_{min} = 0.05\,\text{m}$. To determine the residence time τ_r^* of each tracer in the inter-tidal basin, they are labelled according to their starting position. Each particle is tracked on its path and its residence time is calculated as the time necessary to leave the basin through one of the boundaries. The boundaries of the basin are the eastern and western boundaries of the model domain while the northern boundary is defined as the transition from the basin to the open Wadden Sea in the inlet Accumer Ee located at $y = 7000\,\text{m}$. Tracer particles leaving through

one of the boundaries are not tracked any further and thus cannot enter the domain again. At the end of each model run the mean residence time τ_r for each grid box is computed by averaging over the residence time τ_r^* of the particles it was initialised with. The mean residence time τ_r is obtained as

$$\tau_r(i,j,k) = \sum_{p=1}^{n(i,j,k)} \tau_r^*(i,j,k,p). \tag{4.2.3}$$

By this means, the spatial distribution of the residence time in the basin is calculated. Finally, the residence time maps obtained from all four simulations are averaged to produce the mean residence time map. A similar study has been carried out by *Monsen et al.* [2002] to determine the residence time of Mildred Island, a shallow tidal lake in the Sacramento-San Joaquin River Delta. Particles which are still inside the basin at the end of the simulations are ascribed the model runtime as an estimate of their residence time τ_r^*.
In addition to the four simulations mentioned, a fifth run is carried out to estimate the influence of turbulent diffusion on the spatial distribution of τ_r. The initial conditions are chosen to be the same as for simulation one.

4.2.3 Results

The total number of particles within each water column $N_t(i,j) = \sum_{k=1}^{N} n(i,j,k)$ is shown exemplarily for the first run in Fig. 4.2.1. It is apparent that the particle concentration is higher in the tidal channel and decreases towards the shallow mud flats. The maximum total number of particles in a water column varies throughout the simulations between 760 and 790. The initial conditions for each model run is shown in Tab. 4.2.1. In addition the transport and the water depth in the model domain is shown in Fig. 4.2.3 and Fig. 4.2.4 for maximum ebb and maximum flood stream, respectively. Simulation 1 is carried out under ebb tide conditions and the water leaves the basin with a maximum transport through the deep, narrow inlet of approximately $12.66\,\mathrm{m}^2/\mathrm{s}$ while most of the transport inside the basin is less than $1.15\,\mathrm{m}^2/\mathrm{s}$. The water depth D at the beginning of the first simulation is depicted in Fig. 4.2.3a. The lower part of the basin already shows tidal flats which are dry while most of the basin has a water depth shallower than 2 m. At the end of the simluation a number of 9665 particles is still inside the basin. The corresponding particle distribution is shown in Fig. 4.2.2. The majority of these particles are located in areas with a topographic height less than 2 m in front of the coastline or in the shallow regions behind the barrier islands. It should be stressed here, that these particles are not stuck at horizontal or vertical boundaries but are still in movement.

The vertically averaged residence time map computed from this model run is shown in Fig. 4.2.5a. As would be expected, areas close to the open boundaries of the basin are drained faster than areas closer to the coast. Approximately 50% of the basin volume has a residence time shorter than 2 tidal periods. The residence time is increasing towards shallow regions where the influence of the tidal channels diminishes. In addition to the depth average, the standard deviation of the residence time is calculated and presented as a horizontal plot (see Fig. 4.2.6). The deviation from the mean is especially high in areas with a long residence time which leads to the conclusion that the residence time is depending on the vertical coordinate. In order to show this inhomogenity, the vertical distribution of the residence time along transects across the basin in x- and y-direction, respectively, is displayed in Fig. 4.2.7a and b. The transects are located at $y = 4000\,\mathrm{m}$ (Fig. 4.2.7a) and at $x = 8000\,\mathrm{m}$ (Fig. 4.2.7b). The heterogeneity is higher in shallow areas and decreases towards the deeper parts of the basin. At certain locations the difference between the minimum and maximum residence time ranges up to 6 tidal periods.

The initial conditions for the second simulation are depicted in Fig. 4.2.4. They can be clearly identified as ebb tide conditions. Again, the maximum transport occurs in the inlet of the basin ($12.66\,\mathrm{m}^2/\mathrm{s}$). The distribution of the water depth shows that still some of the mud flats are dry. The residence time map created from this run is shown in Fig. 4.2.5b. The result is not too different from the first simulation. Once more, it can be seen that in the shallow regions the residence time strongly depends on the vertical position in the basin by looking at the standard deviation (see Fig. 4.2.6b). The vertical distribution is similar to the inhomogenity from the first simulation and thus is not discussed any further.

The results from simulation 3 and 4 confirm the results from the first and second run, respectively. Therefore a detailed discussion is not necessarily required.

Finally, the mean residence time map is computed from the results of all four model runs. The distribution of the mean residence time is depicted together with the standard deviation in Fig. 4.2.9.

In a fifth simulation, the influence of the turbulent diffusion on the residence time of the tracer particles τ_r^* is analysed. This experiment is carried out under the same initial conditions as for the first model run, but in this simulation, the turbulent diffusion is not included in the model and transport is only due to advection. While the horizontal distribution of the residence time is similar to the experiments including diffusion, there is a significant difference in the vertical distribution. Exemplarily, the heterogeneity of the

	starting time	starting conditions	n_{total}	V_0	V_t
Simulation 1	19^{th} May 2000, 2:15 am	max. ebb current	153520	141.65	922.66
Simulation 2	19^{th} May 2000, 8:07 am	max. flood current	179140	170.47	951.60
Simulation 3	19^{th} May 2000, 2:21 pm	max. ebb current	155190	143.25	923.07
Simulation 4	19^{th} May 2000, 8:29 pm	max. flood current	176320	167.18	948.15

Table 4.2.1: Initial conditions for the simulations carried out to determine the residence time of the Langeoog basin. The total number of tracer particles used to label the volume of the water masses in the basin V_0 is denoted by n_{total}. V_t is the volume one tracer particle accounts for.

residence time is shown for the same cross sections used for simulation 1. In contrast to the cross sectional plots from the first simulation (see Fig. 4.2.7a), the residence time increases with decreasing depth such that grid boxes close to the bottom have a longer residence time than grid boxes above. This distinct layering which can best be seen in the deeper tidal channels of the basin is shown in detail in Fig. 4.2.8. Thus, it can be concluded, that vertical turbulent diffusion is an important parameter, which cannot be neglected when modelling time scales in shallow water sea areas.

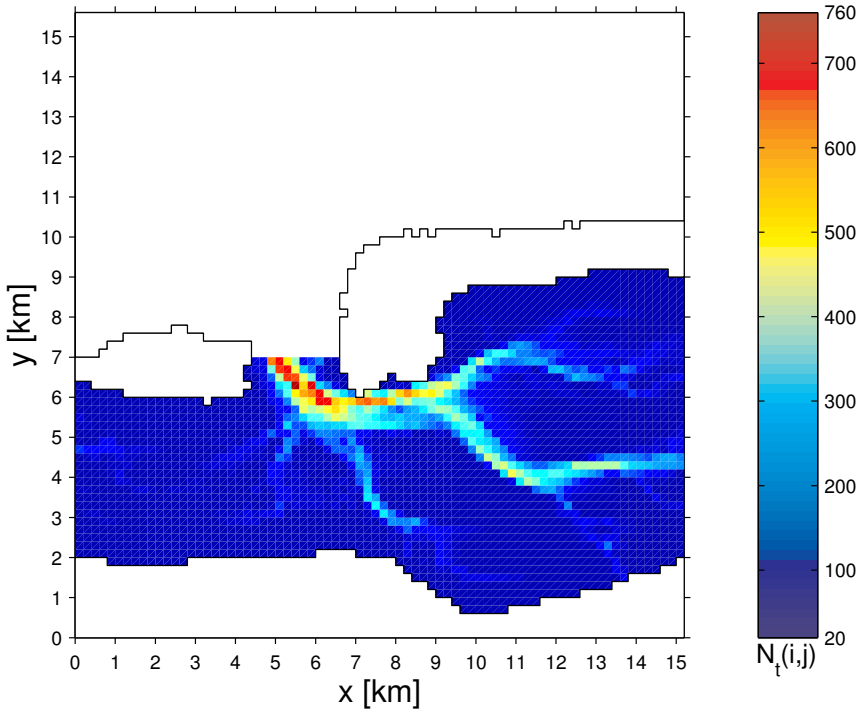

Fig. 4.2.1: Initial horizontal particle distribution $N_t(i,j)$ for simulation 1 under ebb tide conditions. Since initialisation is done under consideration of the volume of the grid boxes, the maximum value of $N_t(i,j)$ is in the deeper part of the inlet.

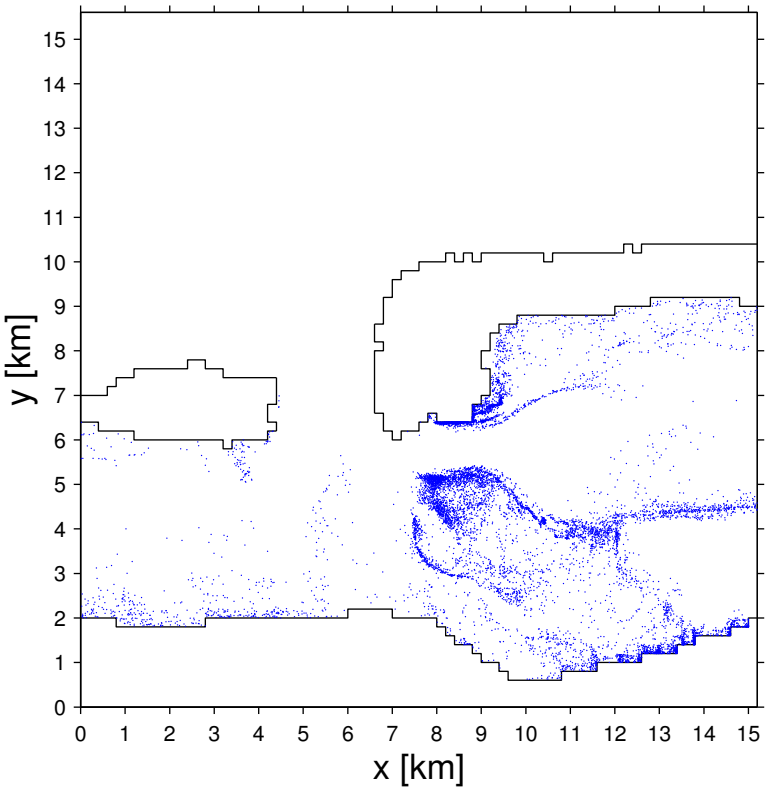

Fig. 4.2.2: Shown is the tracer distribution at the end of the first simulation after $\approx$ 18 tidal periods. A total number of 9665 particles still resides in the basin. The majority of the particles is located in the shallow regions oft the basin, while the tidal channel is completely depleted of particles.

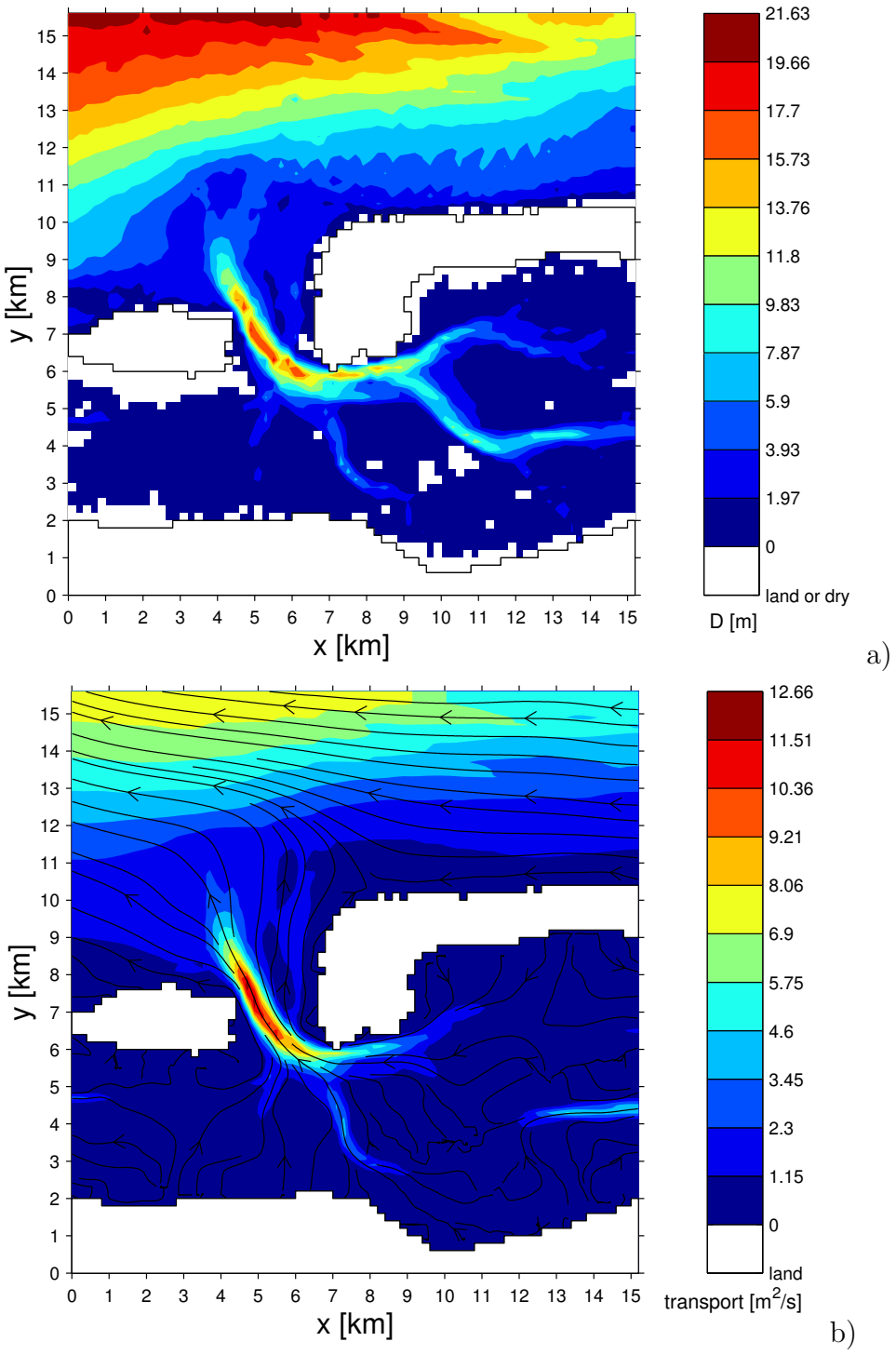

Fig. 4.2.3: a) Water depth and b) transport at the start of simulation 1 under ebb tide conditions. As the basin is drained of water through the tidal channels and the open boundaries to the east and west, the mud flats begin to fall dry. The maximum transport of water is observed in the deeper parts of the basin between the islands. The transport in the shallow regions of the basin is less than $1.15\,\mathrm{m}^2/\mathrm{s}$.

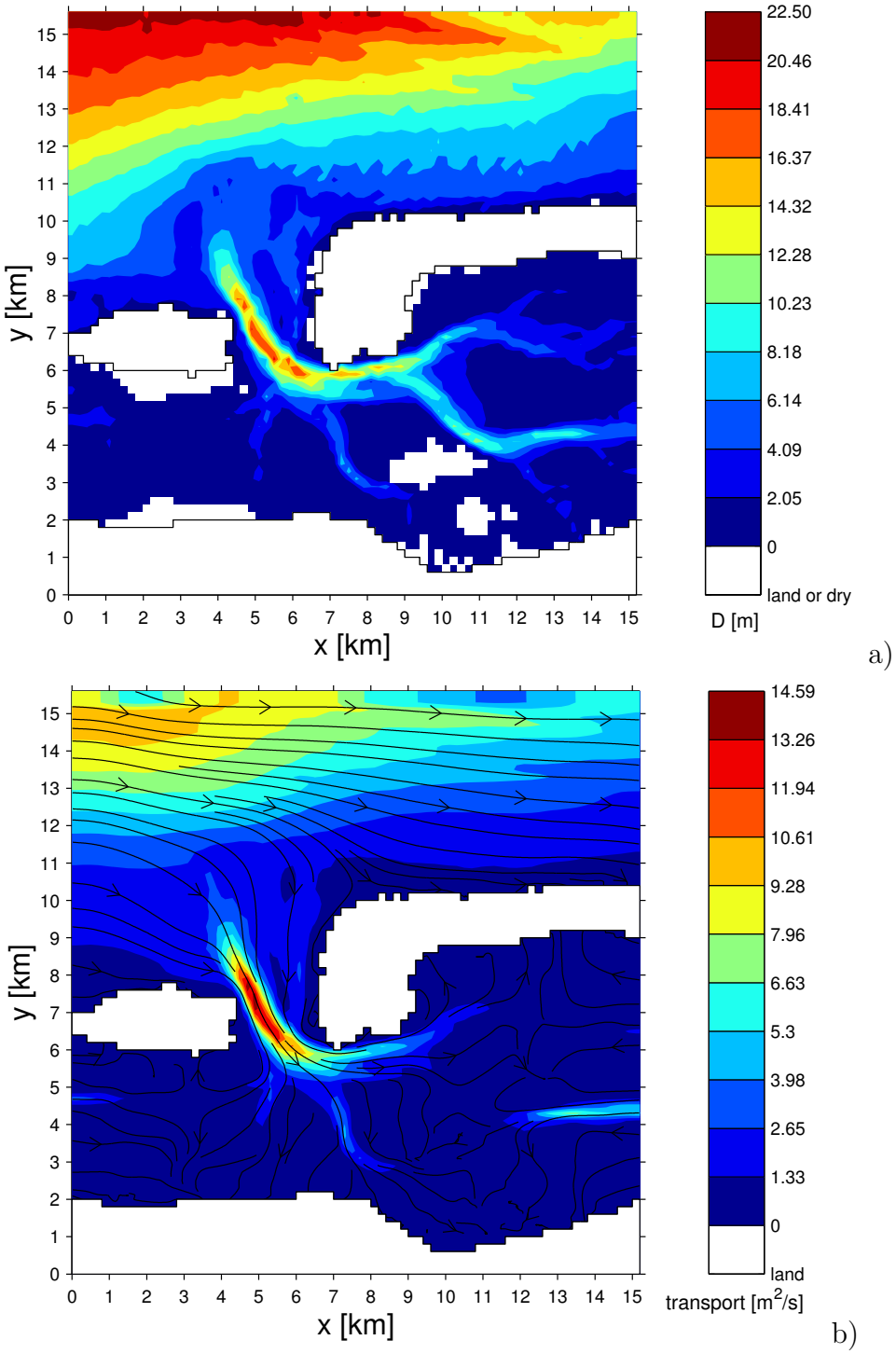

Fig. 4.2.4: a) Water depth and b) transport at the start of simulation 2 under flood tide conditions. Water masses are entering the basin through the inlet and the open boundaries. The maximum transport of water is observed in the deeper parts of the basin between the islands.

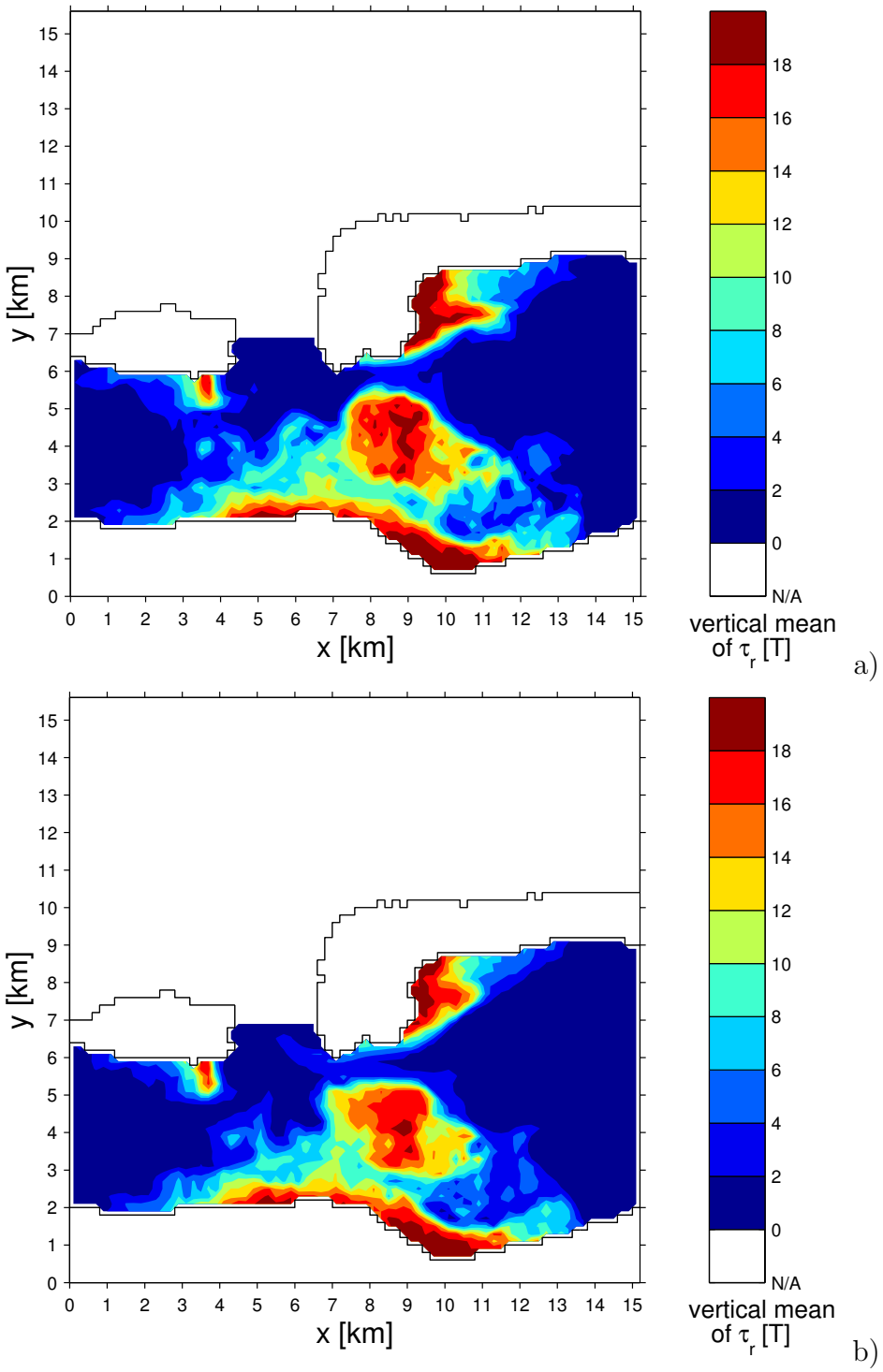

Fig. 4.2.5: Shown is the vertical mean of the residence time τ_r under a) ebb tide conditions and b) flood tide conditions. Both maps are not too different from each other. The residence time is higher in shallow areas and tends to a minimum towards the open boundaries.

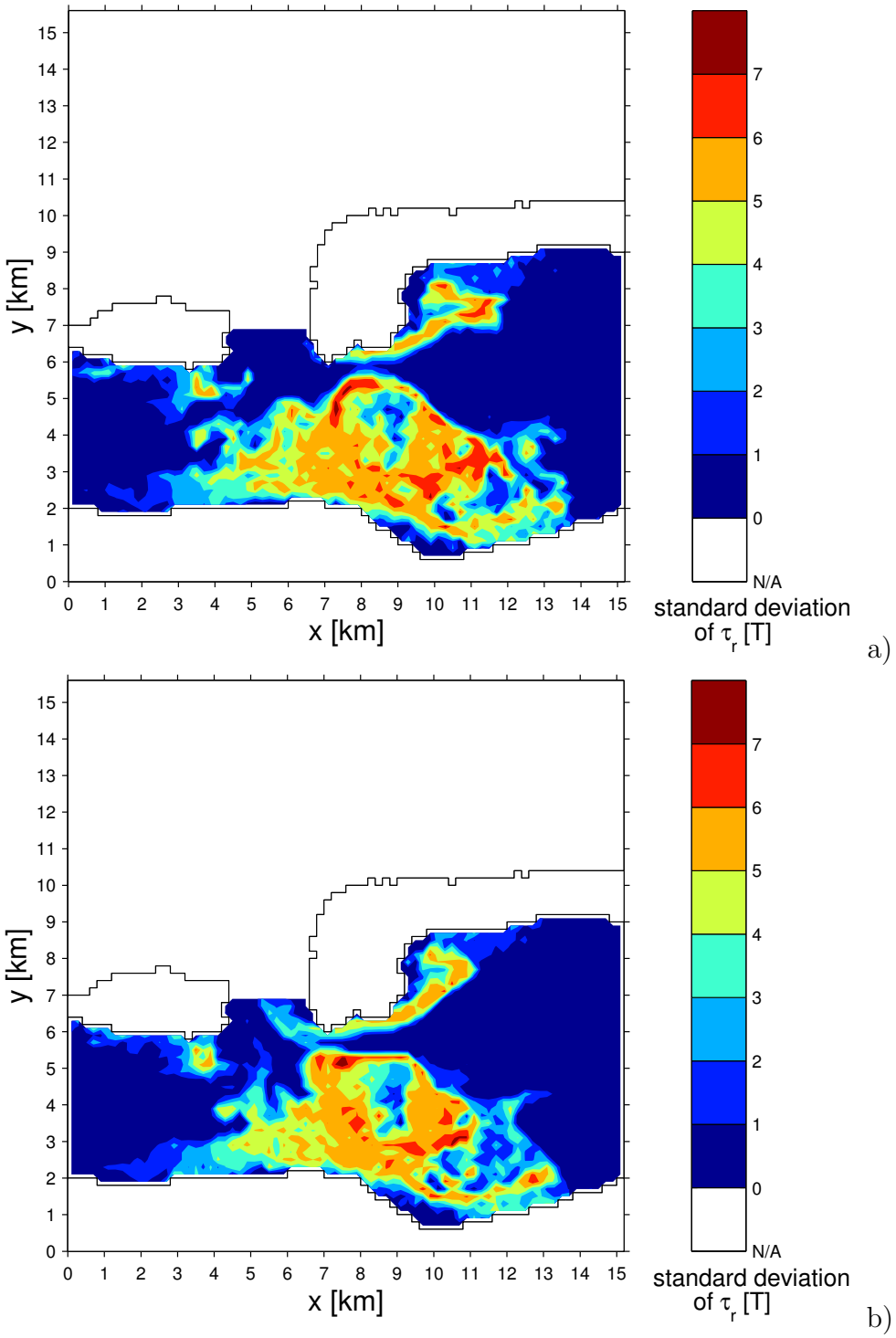

Fig. 4.2.6: Shown is the standard deviation of the residence time τ_r under a) ebb tide conditions and b) flood tide conditions. Both maps are not very different from each other. The standard deviation is higher in shallow water areas with a high residence time.

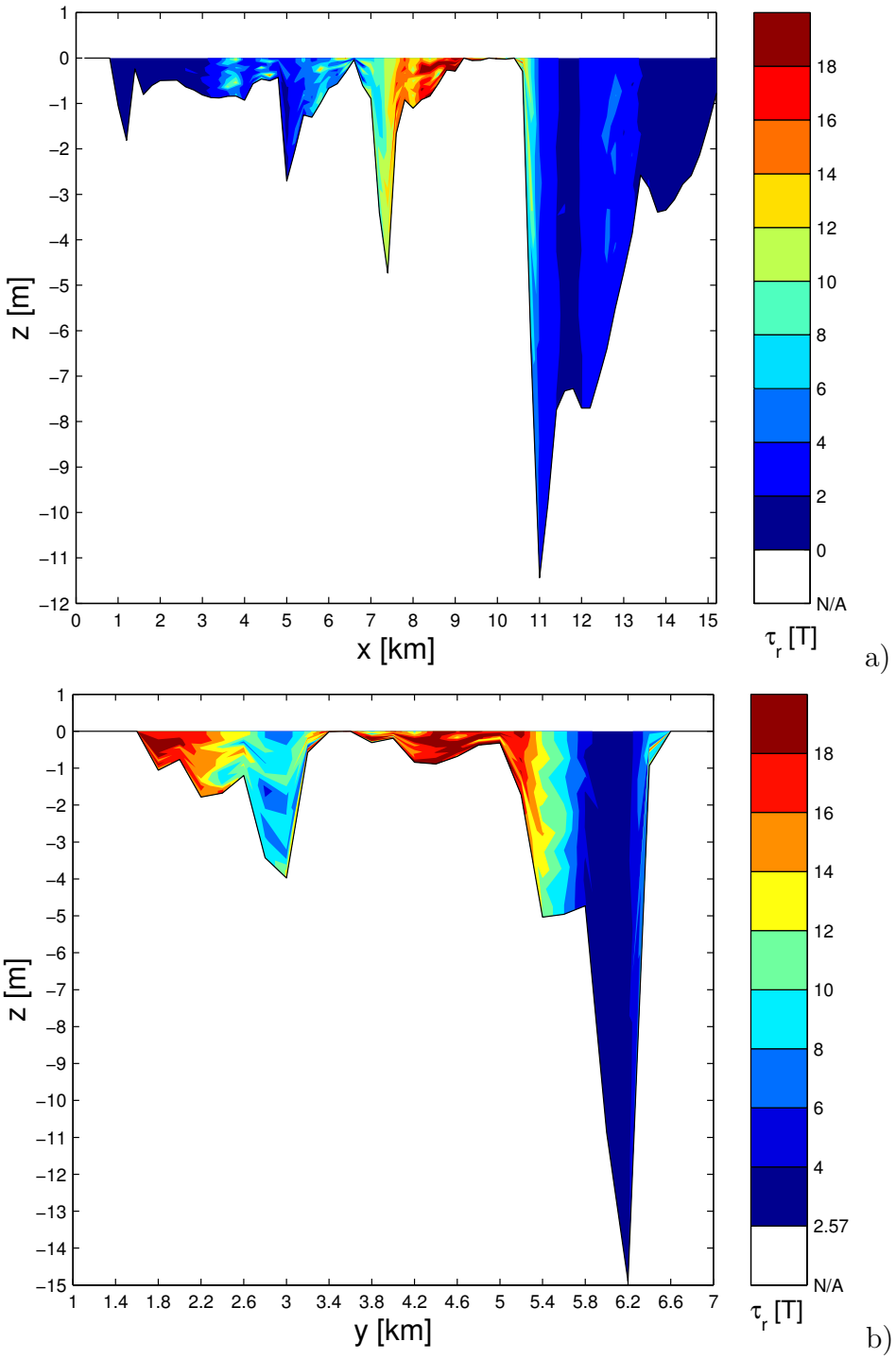

Fig. 4.2.7: Shown is the vertical distribution of the residence time along two transects located at a) $y = 4000\,\mathrm{m}$ and b) $x = 8000\,\mathrm{m}$ for simulation 1. The heterogeneity is higher in shallow areas and decreases towards the deeper parts of the basin. At certain locations the difference between the minimum and maximum residence time ranges up to 6 tidal periods.

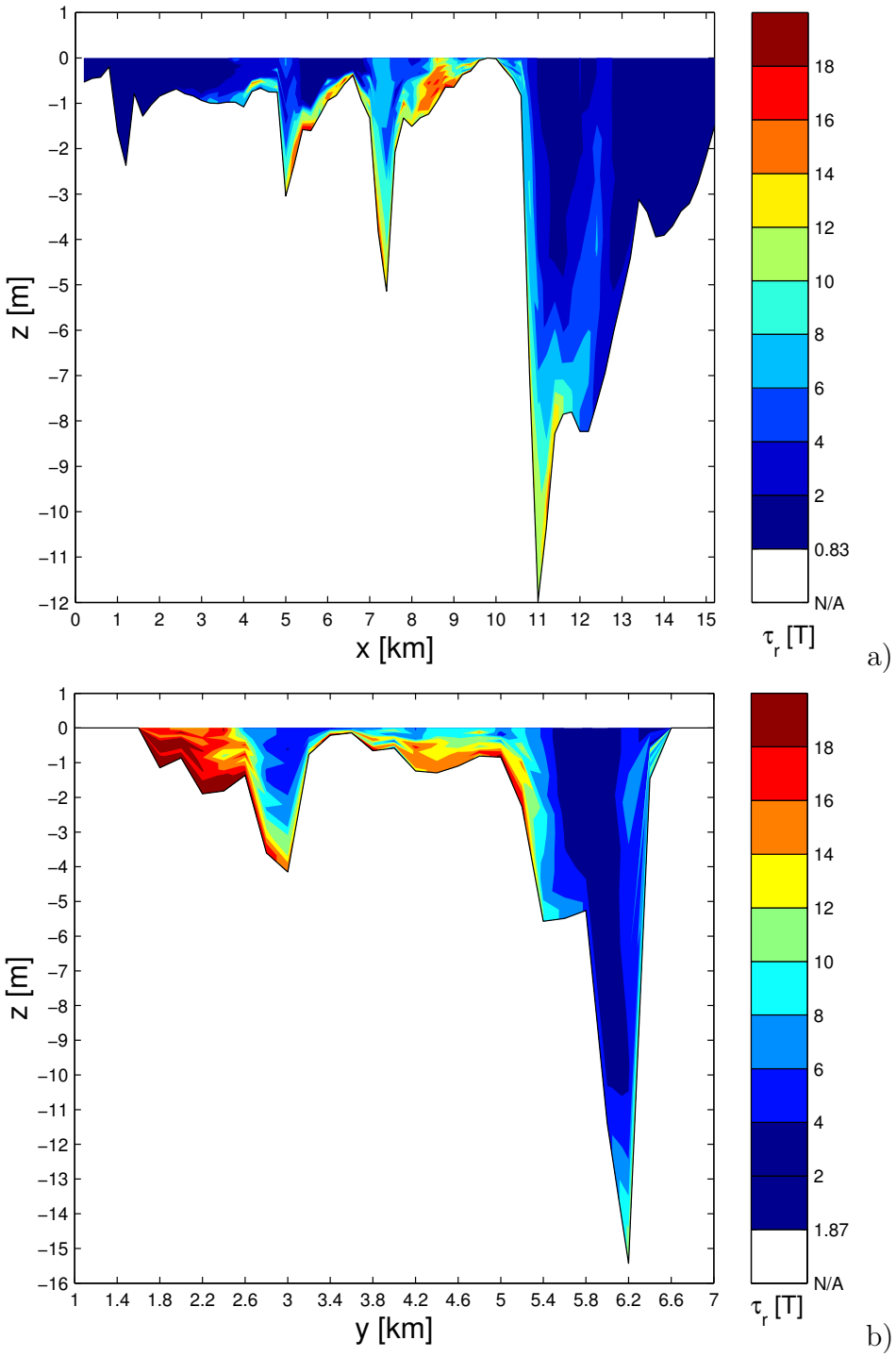

Fig. 4.2.8: Shown is the vertical distribution of the residence time along two transects located at a) $y = 4000\,\mathrm{m}$ and b) $x = 8000\,\mathrm{m}$ for a simulation in which turbulent diffusion is neglected. In contrast to Fig. 4.2.7 the vertical distribution shows signs of layering, such that the residence time increases continuously with depth.

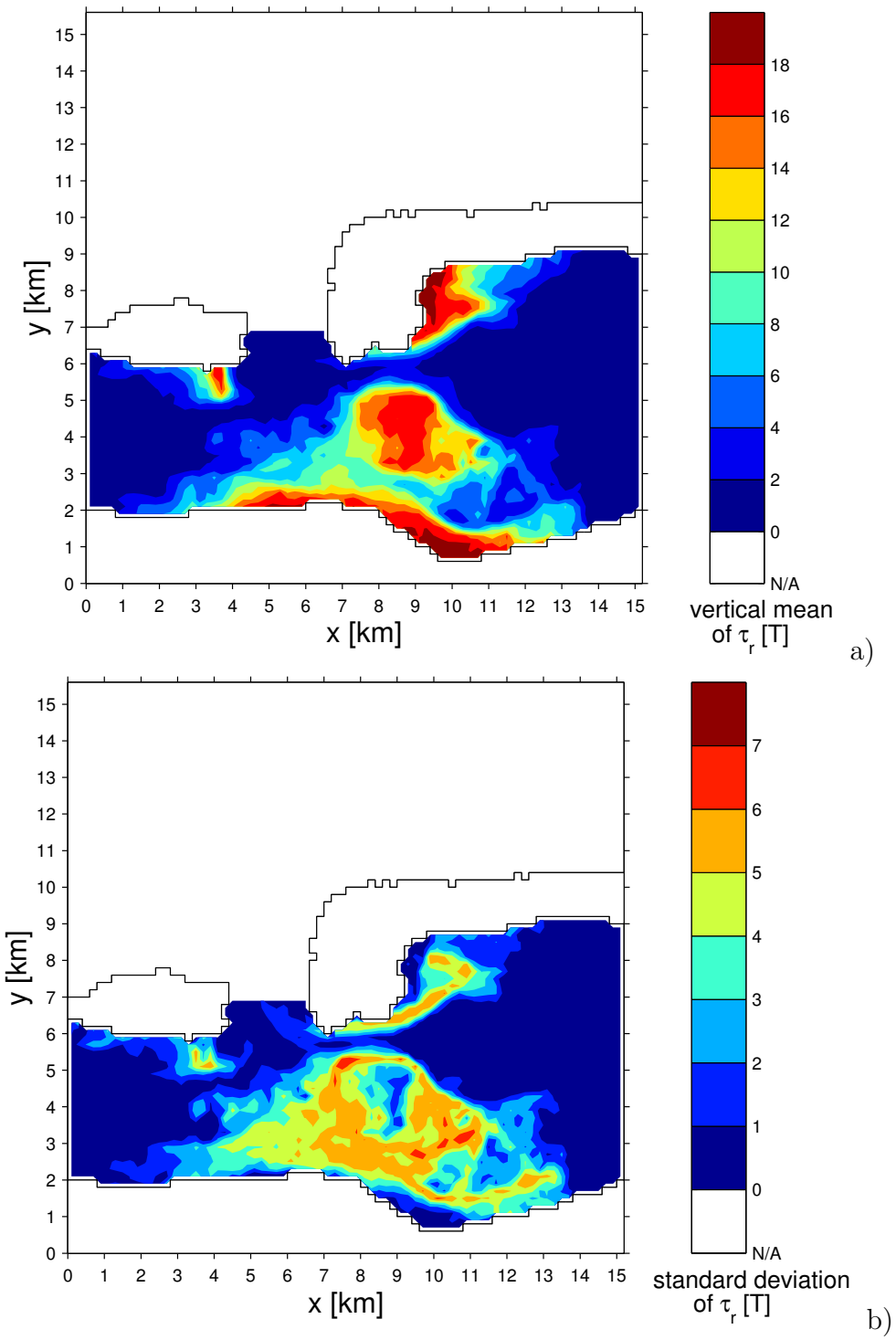

Fig. 4.2.9: Map of the vertically averaged residence time and its standard deviation computed from all simulations. The result is very similar to the maps obtained from the single simulations.

Chapter 5

Summary and outlook

In this study, it was shown how a Lagrangian particle tracking model was implemented into the General Estuarine Transport Model (GETM). The numerics and the physics of the transport model (GETM) were introduced in chapter two together with the advection-diffusion equation and the way it was implemented as a Lagrangian transport model.
In chapter three, the results from the idealised test cases were presented. These test cases ranged from a simple two-dimensional rotation to one- and two-dimensional test cases carried out with GETM and GOTM under idealised conditions.
Finally, the spatial distribution of the residence time in the Langeoog basin was computed with the Lagrangian tracer model. This was achieved by time averaging over four simulations which were carried out within the first day of the time series of the tidal forcing. The averaging was carried out to include both, the influence of the maximum ebb and flood current. Each of the four simulations was carried out with a number of tracer particles representing the initial water volume in the basin. It turned out that the residence time is strongly depending on spatial position. The vertical heterogeneity of the residence time was exemplarily shown and the difference between a model run only with advection and one with advection and diffusion was described.

As an outlook, the work with the Lagrangian tracer model is not finished. I will continue to update it in order to make it releasable at some point in the future. An application of the Lagrangian particle tracking model will be carried out by Hans Burchard and Karsten Bolding as a part of the OCEANIDES project (`http://intelligence.jrc.cec.eu.int/oceanides/-oceanides.html`). The OCEANIDES project aims to improve considerably the monitoring of European seas of illicit marine oil pollution. It is one of

their aims to apply a state-of-the-art dispersion model in combination with an environmental impact assessment model to determine the fraction of oil that is most likely to reach environmentally sensitive areas and the scale of their environmental impact.

Appendix A

Appendix to Section 3.1.1

In this section the analytical solution of the tracer trajectories in the velocity field used for the test case in section 3.1 is derived.
The two-dimensional velocity field is defined by the components u, v of the velocity vector $\vec{v}$ according to

$$u = cx + \omega y \tag{A.0.1}$$

$$v = -\omega x - cy \; . \tag{A.0.2}$$

Here, x and y are the dimensions in space, ω is the angular velocity $\frac{2\pi}{s}$ and $c = \frac{1}{2}\omega$ is a constant. The trajectory of a particle being advected in the velocity field above can be described by the following differential equation

$$\tan\alpha = \frac{dy}{dx} = \frac{v}{u} = \frac{-\omega x - cy}{cx + \omega y} \; , \tag{A.0.3}$$

where α denotes the angle between $\vec{v}$ and the positive x-axis, so that $\tan\alpha$ is the gradient in each point of a trajectory in the velocity field (see Fig. A.0.1). To solve (A.0.3), it is rewritten as a homogeneous differential equation $\frac{dy}{dx} = f(\frac{y}{x})$

$$\frac{dy}{dx} = \frac{-\omega - c\frac{y}{x}}{c + \omega\frac{y}{x}} \tag{A.0.4}$$

and a substitution is carried out by introducing $z(x) = \frac{y}{x}$ with $\frac{dy}{dx} = z + x\,\frac{dz}{dx}$. Hence, (A.0.4) becomes

$$z + x\,\frac{dz}{dx} = \frac{-\omega - cz}{c + \omega z} \; . \tag{A.0.5}$$

In a next step, the variables x, z of (A.0.5) are separated

$$\frac{dx}{x} = \frac{c + \omega z}{-\omega - 2cz - \omega z^2}\, dz \tag{A.0.6}$$

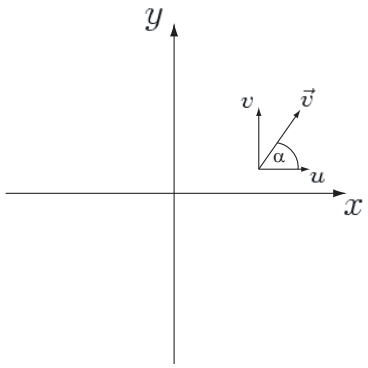

Fig. A.0.1: Illustration of the x,y-coordinate system, the velocity vector $\vec{v}$ with its components u, v and the gradient angle α.

and both sides of the equation are integrated

$$\begin{aligned}
\int \frac{dx}{x} &= -\frac{1}{2} \int \frac{-c-\omega z}{-\frac{1}{2}\omega - cz - \frac{1}{2}\omega z^2}\, dz \qquad \text{(A.0.7)}\\
&\Leftrightarrow \quad \ln|x| = -\frac{1}{2}\, \ln\left|-\frac{1}{2}\omega - cz - \frac{1}{2}\omega z^2\right| + C_1\\
&\Leftrightarrow \quad \ln\left|C_2 x\sqrt{-\frac{1}{2}\omega - cz - \frac{1}{2}\omega z^2}\,\right| = 0\\
&\Leftrightarrow \quad C_2 x\sqrt{-\frac{1}{2}\omega - cz - \frac{1}{2}\omega z^2} = 1\\
&\Leftrightarrow \quad -\frac{1}{2}\omega x^2 - czx^2 - \frac{1}{2}\omega z^2 x^2 = \frac{1}{C_3}\ .
\end{aligned}$$

The back substitution $z = \frac{y}{x}$ yields (with $c = \frac{1}{2}\omega$ and $\omega = 2\pi$)

$$x^2 + xy + y^2 = -\frac{1}{\pi C_3} = \frac{1}{C_4} = C_5\ . \qquad \text{(A.0.8)}$$

The general solution (A.0.8) to (A.0.3) is a quadratic curve. The geometric form of this curve (ellipse, parabola, hyperbola) can be determined by writing (A.0.8) in matrix form and rotating the principal axes around its origin to transform (A.0.8) into a simple sum of squares

$$x^2 + xy + y^2 = \underbrace{(x\ \ y)\begin{pmatrix} 1 & \frac{1}{2} \\ \frac{1}{2} & 1 \end{pmatrix}\begin{pmatrix} x \\ y \end{pmatrix}}_{\vec{x}^T\ A\ \vec{x}} = C_5\ . \qquad \text{(A.0.9)}$$

The transformation of the principal axes is done with a rotary matrix B whose columns consist of the unit eigenvectors $\vec{x}_1, \vec{x}_2$ of A, so that

$$\underbrace{\begin{pmatrix} y_2 & y_1 \\ x_2 & x_1 \end{pmatrix} \begin{pmatrix} 1 & \frac{1}{2} \\ \frac{1}{2} & 1 \end{pmatrix} \begin{pmatrix} x_1 & x_2 \\ y_1 & y_2 \end{pmatrix} = \begin{pmatrix} \lambda_1 & 0 \\ 0 & \lambda_2 \end{pmatrix}}_{B^T A B = D} \tag{A.0.10}$$

where D is a diagonal matrix with the eigenvalues λ_1, λ_2 of A. Any vector $\vec{x}$ can then be represented by a vector $\vec{x}\,'$ out of the transformed coordinate system in the following way

$$\vec{x} = B\vec{x}\,' \,. \tag{A.0.11}$$

The eigenvalues of A are calculated from the characteristic polynomial

$$\det(A - \lambda I) = 0 \Leftrightarrow \det \begin{pmatrix} 1-\lambda & \frac{1}{2} \\ \frac{1}{2} & 1-\lambda \end{pmatrix} = 0$$

to $\lambda_1 = \frac{1}{2}$, $\lambda_2 = \frac{3}{2}$ with the corresponding unit eigenvectors being determined by

$$\begin{aligned} A\vec{x}_1 &= \lambda_1 \vec{x}_1 \\ A\vec{x}_2 &= \lambda_2 \vec{x}_2 \end{aligned}$$

to be

$$\begin{aligned} \vec{x}_1 &= \frac{1}{\sqrt{2}} \begin{pmatrix} 1 \\ -1 \end{pmatrix} \\ \vec{x}_2 &= \frac{1}{\sqrt{2}} \begin{pmatrix} 1 \\ 1 \end{pmatrix} . \end{aligned}$$

Thus the rotary matrix B is

$$B = \frac{1}{\sqrt{2}} \begin{pmatrix} 1 & 1 \\ -1 & 1 \end{pmatrix} . \tag{A.0.12}$$

With the transformation of the principal axes according to (A.0.11), equation (A.0.8) can be written as

$$\begin{aligned} x^2 + xy + y^2 &= \underbrace{\frac{1}{2} (x' \;\; y') \begin{pmatrix} 1 & -1 \\ 1 & 1 \end{pmatrix} \begin{pmatrix} 1 & \frac{1}{2} \\ \frac{1}{2} & 1 \end{pmatrix} \begin{pmatrix} 1 & 1 \\ -1 & 1 \end{pmatrix} \begin{pmatrix} x' \\ y' \end{pmatrix}}_{\vec{x}\,'^T B^T A B \vec{x}\,'} \\ &= \frac{1}{2} x'^{\,2} + \frac{3}{2} y'^{\,2} = C_5 \\ &= x'^{\,2} + 3y'^{\,2} = C_6 \end{aligned} \tag{A.0.13}$$

yielding the equation of an ellipse centred at the origin of the transformed x', y'-coordinate system. The constant of integration C_6 is defined by the initial condition $y(x_0) = y_0$ to be $C_6 = x_0'^2 + 3y_0'^2$, so that (A.0.13) is fully determined

$$\frac{x'^2}{x_0'^2 + 3y_0'^2} + \frac{y'^2}{\frac{1}{3}x_0'^2 + y_0'^2} = 1 \; . \tag{A.0.14}$$

The principle axes of the ellipse (A.0.14) are $a = \sqrt{x_0'^2 + 3y_0'^2}$ and $b = \sqrt{\frac{1}{3}x_0'^2 + y_0'^2}$. According to this, the circumference of the ellipse depends on the starting point (x'_0, y'_0) of a tracer.
The transformation by the rotary matrix B yields a rotation of the ellipse (A.0.14) around the origin of the x', y' coordinate system with an angle ϕ. This angle can be derived from the transformation of the x', y'-coordinates after (A.0.11)

$$\begin{aligned} x &= \frac{1}{\sqrt{2}}(x' + y') \Leftrightarrow x' = \frac{1}{\sqrt{2}}(x - y) \\ y &= \frac{1}{\sqrt{2}}(-x' + y') \Leftrightarrow y' = \frac{1}{\sqrt{2}}(x + y) \; . \end{aligned}$$

The position of the $x'y'$-axes in relation to the axes of the x, y-space can be deduced from $y' = 0 \Leftrightarrow x = -y$ and $x' = 0 \Leftrightarrow x = y$. Hence, the x'- and y'-axis mark the second and the first bisecting line of the x, y-coordinate system. This equals a clockwise rotation of the x, y-axes with the angle $\phi = 45°$ to map them to these axes of the x', y' space. Therefore (A.0.8) describes

$$x^2 + x\,y + y^2 = C_5 = \frac{1}{2}C_6 = \frac{1}{2}x_0'^2 + \frac{3}{2}y_0'^2 = x_0^2 + x_0\,y_0 + y_0^2 \tag{A.0.15}$$

an ellipse which is rotated clockwise with $\phi = 45°$ (Fig. A.0.2).

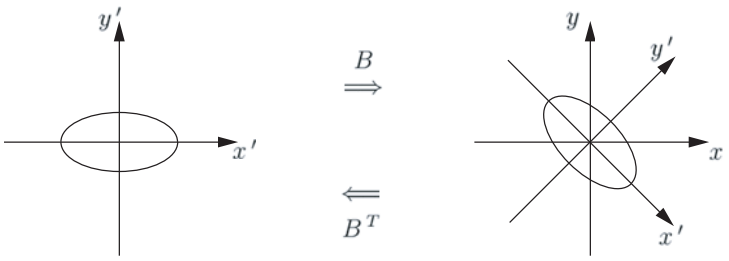

Fig. A.0.2: Illustration of the coordinate systems with the corresponding ellipses. Transformation between the coordinate systems is done with the rotary matrix B and B^T, respectively.

Appendix B

Appendix to Section 2.4.1.2

In the following it is shown how to derive Eq. (2.4.12) in a different way than presented in section 2.4.1.2. Initially the length $\Delta x(t)$ of the path of a particle in x-direction during the time interval Δt can be expressed as a Taylor series about the starting position $x(t_0)$

$$\begin{aligned}\Delta x(t) &= x(t_0+\Delta t) - x(t_0) = \left.\frac{dx}{dt}\right|_{t=t_0} \Delta t + \frac{1}{2}\left.\frac{d^2x}{dt^2}\right|_{t=t_0} (\Delta t)^2 \\ &+ \left.\frac{1}{3!}\frac{d^3x}{dt^3}\right|_{t=t_0} (\Delta t)^3 + \cdots\end{aligned} \tag{B.0.1}$$

Recognising that the velocity of the tracer at any position x is

$$\frac{dx}{dt} = \frac{x-x_l}{x_r-x_l}u_r + \left[1 - \frac{x-x_l}{x_r-x_l}\right] u_l = x\frac{\Delta u}{\Delta x} - x_l\frac{\Delta u}{\Delta x} + u_l = u. \tag{B.0.2}$$

one can replace all terms on the right-hand side of Eq. (B.0.1). The first term of the Taylor series is simply

$$\left.\frac{dx}{dt}\right|_{t=t_0} = x\frac{\Delta u}{\Delta x} - x_l\frac{\Delta u}{\Delta x} + u_l = u_0 \tag{B.0.3}$$

and the following terms can be written as

$$\begin{aligned}\left.\frac{d^2x}{dt^2}\right|_{t=t_0} &= \left.\frac{d}{dt}\left(x\frac{\Delta u}{\Delta x} - x_l\frac{\Delta u}{\Delta x} + u_l\right)\right|_{t=t_0} \\ &= \left.\frac{\Delta u}{\Delta x}\frac{dx}{dt}\right|_{t=t_0} \\ &= u_0\frac{\Delta u}{\Delta x}\end{aligned} \tag{B.0.4}$$

$$\begin{aligned}
\left.\frac{d^3x}{dt^3}\right|_{t=t_0} &= \left.\frac{d^2}{dt^2}\left(x\frac{\Delta u}{\Delta x} - x_l\frac{\Delta u}{\Delta x} + u_l\right)\right|_{t=t_0} \\
&= \left.\frac{\Delta u}{\Delta x}\frac{d}{dt}\left(\frac{dx}{dt}\right)\right|_{t=t_0} \\
&= \left.\frac{\Delta u}{\Delta x}\frac{d}{dt}\left(x\frac{\Delta u}{\Delta x} - x_l\frac{\Delta u}{\Delta x} + u_l\right)\right|_{t=t_0} \\
&= u_0\frac{\Delta^2 u}{\Delta^2 x} \\
&\vdots
\end{aligned} \tag{B.0.5}$$

such that Eq. (B.0.1) becomes

$$\Delta x(t) = u_0\Delta t + u_0\frac{\Delta u}{\Delta x}(\Delta t)^2 + u_0\left(\frac{\Delta u}{\Delta x}\right)^2(\Delta t)^3 + \dots \tag{B.0.6}$$

In a next step Eq. (B.0.6) is rewritten to further simplify it

$$\Delta x(t) = u_0\,\frac{\Delta x}{\Delta u}\left(\underbrace{\frac{\Delta u\;\Delta t}{\Delta x}}_{=y} + \frac{1}{2}\,\underbrace{\frac{(\Delta u\;\Delta t)^2}{\Delta x^2}}_{=y^2} + \frac{1}{3!}\,\underbrace{\frac{(\Delta u\;\Delta t)^3}{\Delta x^3}}_{=y^3} + \cdots\right). \tag{B.0.7}$$

The quantities in brackets are the first, second and third order terms of the Taylor expression of

$$e^y - 1 = \sum_{i=1}^{n}\frac{1}{n!}\,y^n \tag{B.0.8}$$

and the distance a tracer travels during a time step Δt is

$$\Delta x(t) = u_0\,\frac{\Delta x}{\Delta u}\left(e^{\frac{\Delta u}{\Delta x}\Delta t} - 1\right). \tag{B.0.9}$$

The solution for the spatial step in x- and y-direction is in analogy to Eq. (B.0.9) and reads

$$\Delta y(t) = v_0\,\frac{\Delta y}{\Delta v}\left(e^{\frac{\Delta v}{\Delta y}\Delta t} - 1\right) \tag{B.0.10}$$

$$\Delta z(t) = w_0\,\frac{\Delta z}{\Delta w}\left(e^{\frac{\Delta w}{\Delta z}\Delta t} - 1\right) \tag{B.0.11}$$

.

References

Arakawa, A., and V. R. Lamb, Computational design of the basic dynamical processes of the UCLA General Circulation Model, *Meth. Comput. Phys.*, pp. 173–263, 1977.

Burchard, H., Presentation of a new numerical model for turbulent flow in estuaries, in *Hydroinformatics '98*, edited by V. Babovic and L. C. Larsen, pp. 41–48, Balkema, Rotterdam, 1998, Proceedings of the third International Conference on Hydroinformatics, Copenhagen, Denmark, 24-26 August 1998.

Burchard, H., *Applied turbulence modelling in marine waters*, vol. 100 of *Lecture Notes in Earth Sciences*, Springer, Berlin, Heidelberg, New York, 2002.

Burchard, H., and K. Bolding, GETM – a General Estuarine Transport Model. Scientific documentation, *Tech. Rep. EUR 20253 EN*, European Commission, 2002.

Burchard, H., K. Bolding, and M. R. Villarreal, GOTM – a General Ocean Turbulence Model. Theory, applications and test cases, *Tech. Rep. EUR 18745 EN*, European Commission, 1999.

Deleersnijder, E., and B. Tartinville, The radiological situation at the atolls of Mururoa and Fangataufa, *Technical Report, Volume 5: Transport of radioactive material wihtin the marine environment IAEA-MFTR-5*, International Atomic Energy Agency, Austria, 1998.

Dick, S., and W. Schönfeld, Water transport and mixing times in the North Frisian Wadden Sea – Results of numerical investigations, *Deutsche Hydrographische Zeitschrift*, *48*, 27–48, 1996.

Dick, S., and C. S. Soetje, An operational oil dispersion model for the German bight, *Deutsche Hydrographische Zeitschrift*, *Erg.-H Reihe B, Nr. 16*, 43 pp., 1990.

Dimou, K. N., and E. E. Adams, A random-walk, particle tracking model for well-mixed estuaries and coastal waters, *Estuarine, Coastal and Shelf Science*, *37*, 99–110, 1993.

Duwe, K., Modellierung der Brackwasserdynamik eines Tideästuars am Beispiel der Unterelbe, Ph.D. thesis, Department of Geosciences, University of Hamburg, 1988.

Duwe, K. C., J. Krohn, K. D. Pfeiffer, J. C. Riedel-Lorje, and K. C. Soetje, *Ausbreitung von wassergefährdenden Stoffen in der südlichen Deutschen Bucht und im Elbe-Ästuar nach Freisetzung durch Schiffe*, GKSS-Forschungszentrum GmbH, Geesthacht, 1987.

Einstein, A., Über die von der molekularkinetischen Theorie der Wärme geforderten Bewegung von in ruhenden Flüssigkeiten suspendierten Teilchen, *Ann. Phys.*, *549*, 23–35, 1905.

Feller, W., Über den zentralen Grenzwertsatz der Wahrscheinlichkeitsrechnung, *Math. Zeit.*, *40*, 521–559, 1935.

Fischer, H. B., E. G. List, R. C. Y. Koh, and J. Imberger, *Mixing in Inland and Coastal Waters*, Academic Press, New York, 1979.

Freeman, N. G., A. M. Hale, and M. B. Danard, A modified sigma equations approach to the numerical modeling of Great Lakes hydrodynamics, *J. Geophys. Res.*, *77*, 1050–1060, 1972.

Gardiner, C. W., *Handbook of Stochastic Methods for Physics, Chemistry and the Natural Science*, vol. 13 of *Springer Series in Synergetics*, Springer-Verlag, Berlin, Heidelber, New York, Tokyo, 1983.

Haidvogel, D. B., and A. Beckmann, *Numerical Ocean Circulation Modelling*, vol. 2 of *Series on Environmental Science and Management*, Imperial College Press, London, 1999.

Hunter, J. R., P. D. Craig, and H. E. Philips, On the use of random walk models with spatially variable diffusivity, *J. Computat. Phys.*, *106*, 366–376, 1993.

Maier-Reimer, E., Hydrodynamisch-Numerische Untersuchungen zu horizontalen Ausbreitungs- und Transportvorgängen in der Nordsee, Ph.D. thesis, Institute of Oceanography, University of Hamburg, 1973.

Maier-Reimer, E., and J. Sündermann, On tracer methods in computational hydrodynamics, in *Engineering Applications of Computational Hydrodynamics, Vol. 1*, edited by M. Abbot and J. Cunge, pp. 198–217, Pitman, Boston, 1982.

Monsen, N. E., J. E. Cloern, L. V. Lucas, and S. G. Monismith, A comment on the use of flushing time, residence time, and age as transport time, *Limnol. Oceanogr., 47(5)*, 1545–1553, 2002.

Müller-Navarra, S. H., and E. Mittelstaedt, Schadstoffausbreitung und Schadstoffbelastung in der Nordsee, *Deutsche Hydrographische Zeitschrift, Erg.-H Reihe B, Nr. 18*, 51 pp., 1987.

Pietrzak, J., The use of TVD limiters for forward-in-time upstream-biased advection schemes in ocean modeling, *Monthly Weather Review*, *126*, 812–830, 1998.

Press, W. H., S. A. Teukolsky, W. T. Vetterling, and B. Flannery, *Numerical Recipes in FORTRAN 90: The Art of Scientific Computing*, Cambridge University Press, New York, 1996.

QSR 1993, Quality status report of the North Sea, subregion 10: the Wadden Sea, 1993.

Ridderinkhof, H., J. T. F. Zimmerman, and M. E. Philippart, Tidal exchange between the North Sea and Dutch Wadden Sea and mixing time scales of the tidal basins, *NSR*, *25(3)*, 331–350, 1990.

Rouse, H., Modern concepts of the mechanics of turbulence, *Trans. Am. Soc. Civ. Eng.*, *102*, 463–543, 1937.

Schwiderski, E., On charting global ocean tides, *Rev. Geophy. Space Phys.*, *18*, 243–268, 1980.

Schönfeld, W., Numerical simulation of the dispersion of artificial radionuclides in the english channel and the North Sea, *JMS*, *6*, 529 – 544, 1994.

Signell, R. P., and W. R. Geyer, Numerical simulation of tidal dispersion around a coastal headland, in *Residual Currents and Long-term Transport*, edited by R. T. Cheng, pp. 210–222, Springer-Verlag, New York, 1990.

Smith, J. D., and S. R. McLean, Spatially averaged flow over a wavy surface, *J. Geophys. Res.*, *82*, 1735–1746, 1977.

Stanev, E., J.-O. Wolff, H. Burchard, K. Bolding, and G. Flöser, On the circulation in the East Frisian Wadden Sea: Numerical modeling and data analysis, *Ocean Dynamics*, *53(1)*, 27–51, 2003a.

Visser, A. W., Using random walk models to simulate the vertical distribution of particles in a turbulent water column, *Mar. Ecol. Prog. Ser.*, *158*, 275–281, 1997.

Zanke, U., Berechnung der Sinkgeschwindigkeiten von Sedimenten, *Mitteilungen des Franzius-Instituts*, *46*, 231–245, 1977.

Zimmerman, J. T. F., Mixing and flushing of tidal embayments in the western dutch Wadden Sea, *Netherlands Journal of North Sea Research*, *10(2)*, 149–191, 1976.